Reconciling the local galaxy population with damped Lyman alpha cross-sections and metal abundances

Zwaan, M. A.; van der Hulst, J. M.; Briggs, F. H.; Verheijen, M. A. W.; Ryan-Weber, E. V.

Published in:
Monthly Notices of the Royal Astronomical Society

DOI:
10.1111/j.1365-2966.2005.09698.x

Mon. Not. R. Astron. Soc. **364,** 1467–1487 (2005) doi:10.1111/j.1365-2966.2005.09698.x

Reconciling the local galaxy population with damped Lyman α cross-sections and metal abundances

M. A. Zwaan,[1★] J. M. van der Hulst,[2] F. H. Briggs,[3,4] M. A. W. Verheijen[2] and E. V. Ryan-Weber[5]

[1] *European Southern Observatory, Karl-Schwarzschild-Strasse 2, 85748 Garching b. München, Germany*
[2] *Kapteyn Astronomical Institute, PO Box 800, 9700 AV Groningen, the Netherlands*
[3] *Research School for Astronomy & Astrophysics, Mount Stromlo Observatory, Cotter Road, Weston, ACT 2611, Australia*
[4] *Australian National Telescope Facility, PO Box 76, Epping, NSW 1710, Australia*
[5] *Institute of Astronomy, University of Cambridge, Madingley Road, Cambridge CB30HA*

Accepted 2005 September 30. Received 2005 September 21; in original form 2005 April 28

ABSTRACT

A comprehensive analysis of 355 high-quality Westerbork Synthesis Radio Telescope (WSRT) H I 21-cm line maps of nearby galaxies shows that the properties and incident rate of damped Lyman α absorption systems (DLAs) observed in the spectra of high-redshift QSOs are in good agreement with DLAs originating in gas discs of galaxies like those in the $z \approx 0$ population. Comparison of low-z DLA statistics with the H I incidence rate and column density distribution $f(N_{\rm H\,I})$ for the local galaxy sample shows no evidence for evolution in the integral 'cross-section density' $\langle n\sigma \rangle = l^{-1}$ (l = mean free path between absorbers) below $z \approx 1.5$, implying that there is no need for a hidden population of galaxies or H I clouds to contribute significantly to the DLA cross-section. Compared with $z \approx 4$, our data indicate evolution of a factor of 2 in the comoving density along a line of sight. We find that $\mathrm{d}N/\mathrm{d}z(z=0) = 0.045 \pm 0.006$. The idea that the local galaxy population can explain the DLAs is further strengthened by comparing the properties of DLAs and DLA galaxies with the expectations based on our analysis of local galaxies. The distribution of luminosities of DLA host galaxies, and of impact parameters between QSOs and the centres of DLA galaxies, is in good agreement with what is expected from local galaxies. Approximately 87 per cent of low-z DLA galaxies are expected to be fainter than L_*, and 37 per cent have impact parameters less than 1 arcsec at $z = 0.5$. The analysis shows that some host galaxies with very low impact parameters and low luminosities are expected to be missed in optical follow-up surveys. The well-known metallicity–luminosity relation in galaxies, in combination with metallicity gradients in galaxy discs, causes the expected median metallicity of low-z DLAs to be low (∼1/7 solar), which is also in good agreement with observations of low-z DLAs. We find that $f(N_{\rm H\,I})$ can be fitted satisfactorily with a gamma distribution, a single power law is not a good fit at the highest column densities $N_{\rm H\,I} > 10^{21}$ cm^{-2}. The vast majority (≈81 per cent) of the H I gas in the local Universe resides in column densities above the classical DLA limit ($N_{\rm H\,I} > 2 \times 10^{20}$ cm^{-2}), with $N_{\rm H\,I} \sim 10^{21}$ cm^{-2} dominating the cosmic H I mass density.

Key words: surveys – galaxies: ISM – quasars: absorption lines – galaxies: statistics – radio lines: galaxies.

1 INTRODUCTION

How does the cosmological mass density of neutral hydrogen (H I) gas evolve over the history of the universe and what sort of galaxies are responsible for this evolution? Two completely unrelated observational techniques are used to find answers to these questions for the present epoch and at earlier cosmic times. At intermediate and high-redshifts (out to $z \sim 6$), deep optical and ultraviolet (UV) spectra of background quasars are scrutinized to find high column density H I that causes optical depth $\tau_{\rm LL} \gtrsim 1$ blueward of the Lyman limit. In detecting these absorbing systems, their distance is not a limiting factor since the detection depends only on the brightness of the background source against which the absorber is found.

★E-mail: mzwaan@eso.org

However, the nature of the absorbing system is difficult to determine because the absorption spectrum only gives information along a very narrow sightline through the system. Despite the large effort that has been dedicated to identify and characterize the high-redshift absorbers through deep optical imaging, very little is yet known about their properties (e.g. Møller et al. 2002, and references therein).

At $z = 0$, 21-cm emission-line surveys are used to study the high column density H I. Blind surveys with the Arecibo and Parkes radio telescopes have resulted in accurate measurements of the cosmic H I mass density $\Omega_{\rm H\,I}(z = 0)$ (Zwaan et al. 1997; Rosenberg & Schneider 2002; Zwaan et al. 2003, 2005). In contrast to the high-redshift studies, the 21-cm emission-line surveys readily result in measurements of the total H I masses of the detected objects. Furthermore, after follow-up with an aperture synthesis instrument, the three-dimensional H I data cube can be obtained, from which a detailed velocity field and column density map can be derived. Unfortunately, the H I 21-cm hyperfine line is very weak, which limits the studies to the very local Universe ($z < 0.2$). The column densities that routine 21-cm emission-line observations can sense, are the same as those of the highest column density Lyman α (Lyα) absorbers known as Damped Lyα systems (DLAs), with column densities $N_{\rm H\,I} > 2 \times 10^{20}$ cm^{-2}. These are the systems that contain most of the cosmic H I mass (e.g. Wolfe et al. 1986; Lanzetta et al. 1991; Storrie-Lombardi & Wolfe 2000), although there are indications that systems with slightly lower column densities may contribute approximately 20 per cent to $\Omega_{\rm H\,I}$ (Péroux et al. 2005).

The purpose of this paper is to test whether the results from the $z = 0$ 21-cm line surveys and the $z > 0$ UV and optical surveys can be reconciled. This question relates directly to the problem of the origin of DLAs. Traditionally, DLAs were thought to arise in large gaseous discs in the process of evolving to present-day spiral galaxies (Wolfe et al. 1986, 1995). This idea was supported by the fact that the velocity profiles of unsaturated, low-ion metal lines are consistent with rapidly rotating, large thick discs (Prochaska & Wolfe 1997, 1998). Dissenting views do exist, perhaps most notably presented by Haehnelt, Steinmetz & Rauch (1998), who argued that the velocity structure can alternatively be explained by protogalactic clumps coalescing on dark matter haloes (see also Khersonsky & Turnshek 1996; Ledoux et al. 1998). In this view, the DLAs are aggregates of dense clouds with complex kinematics rather than ordered rotating gas discs.

Imaging surveys for DLA host galaxies have so far not resulted in a consistent picture of their properties (Le Brun et al. 1997; Fynbo, Møller & Warren 1999; Kulkarni et al. 2000; Bouché et al. 2001; Warren et al. 2001; Colbert & Malkan 2002; Møller et al. 2002; Prochaska et al. 2002; Chen & Lanzetta 2003; Lacy et al. 2003; Rao et al. 2003). The few successful identifications show that a mixed population of galaxies is responsible for the DLA cross-section. Semianalytical and numerical models of galaxy formation point to sub-L_* galaxies as the major contributors to H I cross-section above the DLA limit (e.g. Kauffmann 1996; Gardner et al. 2001; Nagamine, Springel & Hernquist 2004; Okoshi & Nagashima 2005).

In this paper, we concentrate primarily on cross-section arguments. Burbidge et al. (1977) started the discussion on whether the discs of normal galaxies can explain the incidence rate of absorbers. The method consists of multiplying the space density of galaxies (measured through the optical luminosity function) with the average area of the H I disc above the DLA column density limit. Burbidge et al. (1977) concluded that the mean free path for interception with a galactic disc was too large to account for the number of observed absorbers. Wolfe et al. (1986), Lanzetta et al. (1991), Fynbo et al. (1999), Schaye (2001) and Chen & Lanzetta (2003) use variations of this same simple analytical approach for estimates at high and low z. Although these approaches are useful to gain insight in the problem, a much more direct method is to use real 21-cm column density maps of local galaxies to evaluate the DLA incidence rate. This method was first used by Rao & Briggs (1993) who used Gaussian fits to the radial H I distribution of 27 galaxies as measured with the Arecibo Telescope. Much higher resolution H I maps were used by Zwaan, Briggs & Verheijen (2002) who used Westerbork Synthesis Radio Telescope (WSRT) maps of a volume-limited sample of 49 galaxies in the Ursa Major cluster (Verheijen & Sancisi 2001). A similar study was conducted by Ryan-Weber, Webster & Staveley-Smith (2003) based on 35 galaxies selected from the H I Parkes All Sky Survey (HIPASS) (Meyer et al. 2004), which were observed with the Australia Telescope Compact Array (ATCA). Finally, Rosenberg & Schneider (2003) used low-resolution (∼45 arcsec) Very Large Array maps of their sample of 50 H I-selected galaxies.

With the completion of The Westerbork H I survey of Spiral and Irregular galaxies (WHISP) (van der Hulst, van Albada & Sancisi 2001), we have a much larger sample of galaxies available with a high dynamic range in galaxy properties and observed with a spatial resolution of $\approx 12 \times 12$ arcsec$^2/\sin\delta$. With this sample, the cross-section analysis can be done more accurately and in more detail. This paper is organized as follows. In the following section, we describe the details of the WHISP sample, in Section 3 we summarize surveys for low-z DLA host galaxies and compile a sample of these systems that we use for our comparison with $z = 0$. We calculate the H I column density distribution function in Section 4 and compare the results with the statistics at higher redshifts in Section 5. A comparison of the redshift number density dN/dz between $z = 0$ and higher redshift is given in Section 6. In Section 7, we calculate the probability distribution functions of various parameters of cross-section selected galaxy samples and show that these agree well with results of low-z DLA host galaxy searches. In Section 8, we show that the observed metallicities in DLAs are in good agreement with the expected values if low-z DLAs arise in the gas discs of galaxies typical of the $z = 0$ population. Section 9 summarizes the results. We use $H_0 = 75$ km s^{-1} Mpc^{-1} throughout this paper to calculate distance-dependent quantities.

2 THE WHISP SAMPLE

The incidence rate of high column density H I in the local universe can best be calculated from 21-cm maps of a large sample of galaxies with uniform selection criteria and high spatial resolution. Such a sample is available through WHISP (van der Hulst et al. 2001), an H I survey of some 390 galaxies carried out with the WSRT in the periods 1992–1998 and 2000–2002. The aim of this survey is to obtain maps of the distribution and velocity structure of the H I in a large sample of galaxies, covering all Hubble types from S0 to Im and a considerable range in luminosity. This survey increases the number of well-analysed H I observations of galaxies by an order of magnitude, with the principal goal of investigating the systematics of rotation curves and the properties of the dark matter haloes they trace. First results on the late-type galaxies have been published (Swaters et al. 2002) and a study of the early-type galaxies is on its way (Noordermeer et al. 2004, 2005). Examples of H I maps of nine galaxies used in our analysis are shown in Fig. 1, where the top three galaxies have H I masses of $M_{\rm H\,I} \sim 10^8$ M$_\odot$, the middle three have $M_{\rm H\,I} \sim 10^9$ M$_\odot$ and the bottom three have $M_{\rm H\,I} \sim 10^{10}$ M$_\odot$.

The sample from which WHISP candidates have been selected consists of galaxies in the Uppsala General Catalogue (UGC) of Galaxies (Nilson 1973) that fit the following criteria: (i) B-band

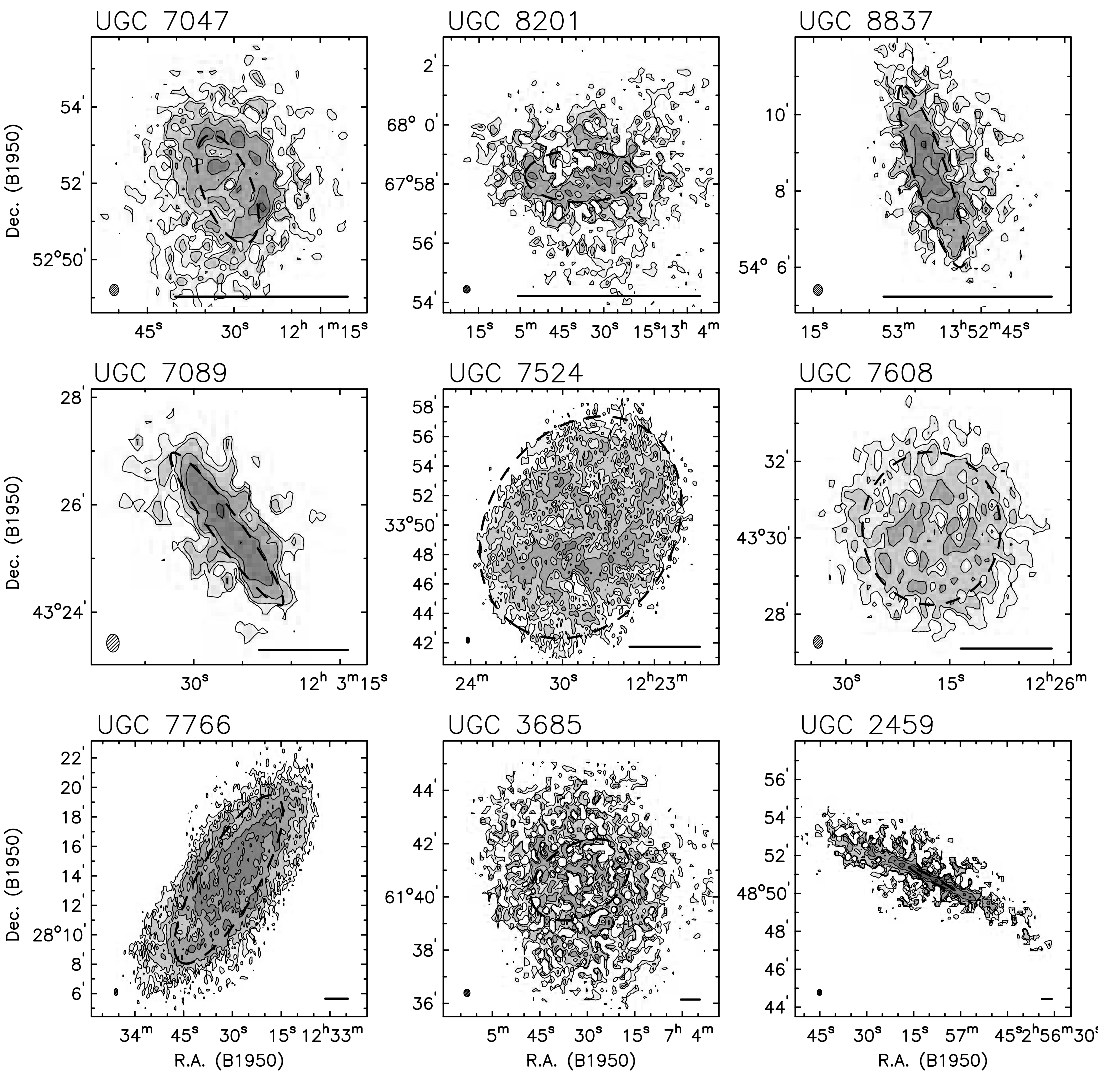

Figure 1. H I column density maps of six of the WHISP galaxies. The top three galaxies have total H I masses of $10^8\,\mathrm{M}_\odot$, the middle three have $M_{\mathrm{H\,I}} \sim 10^9\,\mathrm{M}_\odot$ and the bottom three have $M_{\mathrm{H\,I}} \sim 10^{10}\,\mathrm{M}_\odot$. Contour levels are at column densities of 0.2, 0.5, 1, 2, 4, 8 and 16×10^{21} cm^{-2}, where the lowest contour corresponds to the DLA limit. The beam sizes are indicated in the lower left corners of each panel. The ellipses indicate the orientation parameters of the optical images of these galaxies, and the extent corresponds to the diameter measured at the 25th *B*-magnitude isophote. The scale bar in the lower right corner corresponds to 5 kpc at the distance of the galaxies.

major axis diameter more extended than 1.2 arcmin; (ii) declination (B1950) north of $+20^\circ$ and (iii) the 21-cm flux density averaged over the H I profile exceeds 100 mJy. For observations after the year 2000, the flux density criterion was relaxed to also include galaxies with lower average flux densities. This enabled observation of a reasonably large number of galaxies of Hubble type S0–Sb, which typically have lower H I fluxes than galaxies of Hubble-type Sbc and later. For the analysis presented in this paper, we made use of the data of 355 galaxies out of the total of 391 in the WHISP sample, which had been fully reduced at the time this analysis started. The distribution over Hubble type and optical luminosity for the 355 galaxies in our sample is given in Table 1.

A total of about 4500 h of observing time (more than 1 yr of continuous data taking) was used over a period of 10 yr to observe 391 galaxies. Of these, 281 were observed with the old WSRT system between 1992 and 1998. The remaining 110 galaxies were observed with the upgraded, more sensitive system between 2000 and 2002. The main difference between the two periods is the upgrade of the WSRT with cooled receivers on all telescopes and a greatly improved bandwidth and correlator capacity. In practice, this means that the sensitivity of the observations made in 2000 and thereafter is a factor of $\sim$4 better than before (e.g. a typical rms of 0.8 mJy beam^{-1} as compared to 3 mJy beam^{-1}). The velocity resolution for most galaxies is 5 km s^{-1}. The highly inclined galaxies in the sample with inclinations typically above 60° have been observed at a lower velocity resolution of 20 km s^{-1}, while more face-on galaxies and galaxies with narrow single-dish profiles ($\Delta v \leqslant 60\,\mathrm{km\,s^{-1}}$) have been observed with a velocity resolution of 2.5 km s^{-1}.

The WSRT observations of the WHISP galaxies have been processed following a well-described standard procedure consisting of a (u,v) data-processing phase (data editing, calibration and Fourier transformation) using the native WSRT reduction package NewStar and an image processing phase (continuum subtraction, CLEANing, determination of H I distributions and velocity fields using GIPSY. The resulting data cubes and images have been archived, and a summary is displayed on the web at http://www.astro.rug.nl/~whisp. A precise description of the reduction procedures can also be found there.

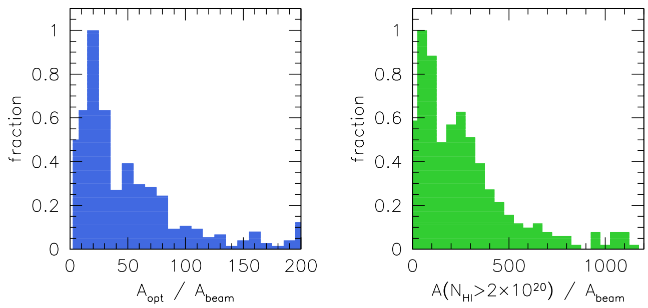

Figure 2. Left-hand panel: Distribution of the number of beams over the optical area within D_{25}. Right-hand panel: Distribution of the number of beams over the area with H I column density exceeding the DLA limit of 2 $\times$ 10^{20} cm^{-2}.

For each observed galaxy, the WHISP pipeline reduction recipe produces data cubes with an angular resolution of $\sim$12 $\times$ 12 arcsec^2/sin δ, 30 $\times$ 30 arcsec^2 and 60$\times$ 60 arcsec ^{2}. The maps with different resolutions are used to obtain some insight in the effect of spatial resolution on the measurement of H I cross sectional areas (see Section 4.1). The median 3σ column density sensitivity limit of the highest resolution H I maps is 2.3 $\times$ 10^{20} cm^{-2}. At the lower resolutions (30 and 60 arcsec^2) the column density sensitivities improve with factors of approximately 3.5 and 10, respectively. To illustrate the resolution of our data, we calculate the total number of beams over the optical area within the 25th magnitude isophote, and the number of beams over the area with an H I column density exceeding the DLA limit. These statistics are presented in Fig. 2. The median number of beams over the optical area is $\approx$40, whereas the median number of beams over the H I area is $\approx$220. We note that the total number of independent H I column density measurements above the DLA limit in our sample is $\approx$140 000.

A possible concern about the selection of the WHISP sample is that the sample is based on the UGC, which implies that the parent sample from which the WHISP galaxies are chosen is optically selected. Since DLAs are purely H I-selected, our $z = 0$ comparison sample of galaxies should ideally also be H I-selected to guarantee that all possible optical selection biases are ruled out. However, Zwaan (2000) has shown that the properties of H I-selected galaxies are not different from those of optically selected galaxies if compared at the same luminosity. Specifically, he showed that the gas richness, optical surface brightness and scalelength of optically selected and H I-selected galaxies are indistinguishable if subsamples with similar median absolute magnitude are compared. Therefore, if the weighting of the sample is properly taken into account (using the luminosity function or H I mass function) no strong biases should be introduced by using optically selected galaxies. As will be discussed in Section 4, we use morphological type-specific H I mass functions to calculate weights for individual galaxies, which will ensure that the morphological-type distribution of our weighted sample at a given H I mass is similar to that of an H I-selected galaxy sample. Small differences in the optical properties of optically and H I-selected samples as a function of H I mass might remain, but given the findings of Zwaan (2000) and the fact that we apply type-specific weighting, these differences are unlikely to bias our results significantly. This is also illustrated by the fact that the value for the redshift number density dN/dz that we derive in Section 6 is consistent with what Ryan-Weber et al. (2003) and Ryan-Weber, Webster & Staveley-Smith (2005a) find based on a smaller sample of H I-selected galaxies.

The field of view of the 21-cm WSRT observations is defined by the diameter of the individual dishes and is approximately 30-arcmin across (at half power beam width). The WHISP data base contains many instances of multiple H I detections within one such field. We separated these multiple detections into individual galaxies if both H I detections could be identified with optically identifiable galaxies in the NASA/IPAC Extragalactic Data base (NED). In most cases, the multiple detections are known pairs or groups of galaxies. If a second H I detection in the field targeted on a UGC galaxy could not be associated with a catalogued galaxy, we did not separate this H I detection but treated it as a companion H I cloud to the known optical galaxy and therefore included it in the total cross-section calculation, keeping information about the impact parameter at which the $N_{\rm H\,I}$ occurs.

All 21-cm maps of the resulting sample of galaxies were transformed to column density maps using the well-known equation

$$N_{\rm H\,I} = 1.823 \times 10^{18} \int T_{\rm B}(v)\,{\rm d}v, \quad (1)$$

where $T_{\rm B}$ is the observed brightness temperature. This equation is valid for optically thin emission. For cold, high column density ($>10^{21}$ cm^{-2}) gas clouds, the optically thin approximation might break down, which would result in slightly underestimated H I column densities. This effect is probably only important for the very highest H I column densities, in the range where there are only very few DLA measurements. Therefore, it is unlikely to affect our comparison between DLAs and local galaxies. Furthermore, the measurement of total cross-sectional area above the DLA column density limit is not affected at all by H I optical depth effects.

3 SEARCHES FOR LOW-Z DLA GALAXIES

The aim of this paper is to make a detailed comparison between the local galaxy population and local DLA galaxies. The difficulty in this comparison is that the number of identified DLA galaxies is very low, at any redshift. There are now approximately 600 DLAs known in the Universe (Prochaska, Herbert-Fort & Wolfe 2005), only $\sim$50 of which are at $z < 1.7$. This number is especially small at low z, because the Lyα line is only observable from the ground when it is redshifted to $z > 1.7$. Furthermore, due to the expansion of the universe, the expected number of absorbers along a line of sight decreases with decreasing redshift, which naturally leads to a scarcity of DLAs at low z.

At high z, there is a substantial number of systems available, but attempts to directly image their host galaxies have generally been unsuccessful (see e.g. Colbert & Malkan 2002; Møller et al. 2002; Prochaska et al. 2002). A few positive identifications do exist, mostly the result of *Hubble Space Telescope* (*HST*) imaging (Fynbo et al. 1999; Kulkarni et al. 2000; Warren et al. 2001; Møller et al. 2002). Possibly, the best data to date are available for three objects imaged with the Space Telescope Imaging Spectrograph by Møller et al. (2002). They found emission from three DLA galaxies with spectroscopic confirmation, and concluded that the objects are consistent with being drawn from the population of Lyman-break galaxies.

Although the absolute number of DLAs at low z is small, the success rate for finding their host galaxies is better for obvious reasons: the host galaxies are expected to be brighter, and the separation on the sky between the bright QSO and the DLA galaxy is likely larger. The first systematic survey for low-z DLA host galaxies was performed by Le Brun et al. (1997), who obtained *HST R*- and *B*-band imaging of seven QSO fields with known DLAs. For most

Table 1. Properties of the WHISP sample.

	$L_B < L_B^*/20$	$L_B^*/20 < L_B < L_B^*/5$	$L_B^*/5 < L_B < L_B^*$	$L_B > L_B^*$	Total
E/S0	2	2	8	9	21
Sa/Sb	4	7	31	41	83
Sbc/Sc	7	14	37	52	110
Scd/Sd	19	15	17	4	55
Sm/Irr	43	31	7	5	86
Total	75	69	100	111	355

of their targets, they found likely galaxies, the properties of which span a large range from low surface brightness (LSB) dwarfs to large spirals. Similar searches for single systems were done by Burbidge et al. (1996) and Petitjean et al. (1996). The DLA at $z = 0.656$ in the sightline towards 3C 336 was studied extensively by Steidel et al. (1997) and Bouché et al. (2001), but despite the deep *HST* imaging in the optical and Hα, no galaxy has been identified. All these studies lacked spectroscopic follow-up, so associations were purely based on the proximity of identified galaxies to the QSO sightline, which is not unique in many cases. Optical and infrared imaging combined with spectroscopic follow-up observations were first done by Turnshek et al. (2001), who successfully identified two galaxies at $z = 0.091$ and 0.221. Using a similar technique, Lacy et al. (2003) also identified two low-z DLA galaxies. Chen & Lanzetta (2003) demonstrated that it is possible to use photometric redshifts to determine the association of optically identified galaxies with DLAs, and applied this technique to six DLAs. Finally, Rao et al. (2003) studied four DLAs, and were able to confirm two DLA galaxies based on spectroscopic confirmation, one using a photometric redshift, and one association was based on proximity to the QSO.

Two attempts have been made to directly measure the cold gas contents of low-z DLAs by means of deep 21-cm emission-line observations (Lane, Briggs & Smette 2000; Kanekar et al. 2001). The problem with these observations is that the 21-cm line is extremely weak so that with present technology surveys are limited to the very local ($z < 0.2$) universe. Both observations resulted in non-detections, which allowed the authors to put upper limits to the H I masses of approximately $M_{\mathrm{H\,I}} = 2.3 \times 10^9\ \mathrm{M}_{\odot}$, which is one-third of the H I mass of an L_* galaxy (Zwaan et al. 2003, 2005).

In addition to these surveys for low-z DLA galaxies, there are two cases of high column density absorption systems found in local galaxies. Miller, Knezek & Bregman (1999) and Bowen, Tripp & Jenkins (2001) study the absorption line systems seen in NGC 4203 and SBS 1543+593, at redshifts of 0.004 and 0.009, respectively. For these systems, the galaxy–QSO alignment was identified before the absorption was found, and in one case (NGC 4203) Lyα absorption has not been seen to date, but the structure and strength of observed metal lines resemble those of DLAs.

All together, including the $z \approx 0$ systems NGC 4203 and SBS 1543+593, there are now 20 DLA galaxies known at $z < 1$. Table 2 summarizes the properties of these galaxies. We have been fairly generous in assembling this table because not all listed galaxies have been spectroscopically confirmed. Also, some of the systems fall just below the classical DLA column density limit of $\log N_{\mathrm{H\,I}} = 20.3$,

Table 2. Properties of $z < 1$ (sub-)DLA host galaxies.

QSO	z_{abs}	$\log N_{\mathrm{H\,I}}$ (cm^{-2})	b (kpc)	L/L_*	Morphology	Reference	Redshift[1]
Ton 1480	0.004	20.34	7.9	0.44	Early type	a	Spectro-z
HS 1543+5921	0.009	20.34	0.4	0.02	Early type	b	Spectro-z
Q0738+313	0.091	21.18	<3.1	0.08	LSB	c	No
PKS 0439-433	0.101	20.00	6.8	1.00	Disc	d,g,k	Spectro-z
Q0738+313	0.221	20.90	17.3	0.17	Dwarf spiral	c,g	Spectro-z
PKS 0952+179	0.239	21.32	<3.9	0.02	Dwarf LSB	e	Photo-z
PKS 1127-145	0.313	21.71	<5.6	0.16	Patchy irr LSB[2]	e,g,l	Spectro-z
PKS 1229-021	0.395	20.75	6.6	0.17	Irr LSB	f	No
Q0809+483	0.437	20.80	8.3	2.80	Giant Sbc	f,j,k	Spectro-z
AO 0235+164	0.524	21.70	12.5	1.90	Late-type spiral[2]	g,m	Spectro-z
B2 0827+243	0.525	20.30	29.5	1.04	Disturbed spiral	e,g	Spectro-z
PKS 1629+120	0.531	20.69	14.7	0.78	Spiral	e,g	Spectro-z
LBQS 0058+0155	0.613	20.08	7.5	0.60	Spiral	h,k	Spectro-z
Q1209+107	0.630	20.20	9.7	1.90	Spiral	f	No
HE 1122-1649	0.681	20.45	23.5	0.58	Compact	g	Photo-z
Q1328+307	0.692	21.19	5.7	0.67	LSB	f	No
FBQS 1137+3907C	0.720	21.10	10.3	0.20	Spiral?	i	Spectro-z
FBQS 0051+0041A	0.740	20.40	22.4	0.80	Spiral?	i	Spectro-z
MC 1331+170	0.744	21.17	25.1	3.00	Edge-on spiral	f	No
PKS 0454+039	0.860	20.69	5.5	0.60	Compact	f,j	No

References: (a) Miller et al. (1999); (b) Bowen et al. (2001); (c) Turnshek et al. (2001); (d) Petitjean et al. (1996); (e) Rao et al. (2003); (f) Le Brun et al. (1997); (g) Chen & Lanzetta (2003); (h) Pettini et al. (2000); (i) Lacy et al. (2003); (j) Colbert & Malkan (2002); (k) Chen et al. (2005); (l) Lane et al. (1998) and (m) Burbidge et al. (1996).

[1] Indication of whether the redshift of the DLA galaxy has been confirmed by either spectroscopy or a photometric redshift measurement.

[2] Probably arising in galaxy group.

but we decided to include these because our 21-cm emission-line data are also sensitive below this limit. However, in the remainder of this paper when we refer to 'DLA column densities', we restrict our analysis to $\log N_{\rm H\,I} > 20.3$ and disregard the identified systems with lower column densities. Some systems in our compilation have been studied by several authors, in which case we choose the parameters from the most recent reference. The measurements of L/L_* are mostly based on *B*-band data, but in some cases these data were not available, in which cases we used *K* or *R* band. For the value of L_*, we adopted the recent measurement of $M_B^* - 5\log h_{75} = -20.3$ from Norberg et al. (2002), $M_R^* - 5\log h_{75} = -21.1$ from Lin et al. (1996) and $M_K^* - 5\log h_{75} = -24.1$ from Cole et al. (2001). The morphological classifications are copied directly from the relevant references and are very heterogeneous in their degree of detail. Therefore, we note that the L/L_* values and the listed types should be treated with caution and both parameters have large uncertainties. Our local DLA galaxy sample is defined to have redshifts $z < 1$, which is of course a random choice. However, cutting the sample at lower redshift would result in too small a sample to make a meaningful comparison with our nearby galaxy statistics. The median redshift of the DLA galaxy sample is $\langle z \rangle = 0.5$. In the analysis, we ignore any evolutionary effect in the redshift range $z = 1$ to 0. This assumption is justified by our finding in Section 6 that the cross-section times comoving space density of DLAs is not evolving in this redshift range. However, an important caveat is that this lack of evolution in cross-section puts no constraints on how gas is distributed in individual systems, but only on the total gas content averaged over the whole galaxy population. The mean properties of gas discs in galaxies might evolve since $z = 1$. Given the fact that the cosmic star formation rate density drops by a factor 8 between $z = 1$ and $z = 0$ (e.g. Hopkins 2004), it is possible that the evolution of the neutral gas discs actually takes place as well. To study the H I mass evolution of galaxies deep observations with future instrument such as the Square Kilometer Array (Carilli & Rawlings 2004) are required. At present no observational constraints exist. Apart from the evolution of the H I discs, the optical properties of DLA host galaxies could evolve between $z = 1$ and 0 as well. However, Chen & Lanzetta (2003) find that DLA galaxies do not show luminosity evolution between $z = 1$ and 0, although the constraints are limited by small number statistics.

Finally, one might be concerned about the process of choosing which galaxy to attribute to a certain absorber (see discussion in Chen & Lanzetta 2003). In some cases, more than one candidate is available, in which case the authors are forced to choose which one is the most likely absorber. The set of arguments on which this choice is based varies between different studies. We note that this introduces some randomness in our compilation presented in Table 2.

The conclusion from studying Table 2 is that the sample of low-z DLA galaxies spans a wide range in galaxy properties, ranging from inconspicuous LSB dwarfs to giant spirals and even early-type galaxies. Obviously, it is not just the luminous, high surface brightness spiral galaxies that contribute to the H I cross-section above the DLA threshold, although it is these galaxies that contribute most to the total comoving density $\Omega_{\rm H\,I}$.

4 CALCULATING THE COLUMN DENSITY DISTRIBUTION FUNCTION – $F(N_{\rm H\,I})$

In QSO absorption line studies, the column density distribution $f(N_{\rm H\,I})$ function is defined such that $f(N_{\rm H\,I})\,{\rm d}N_{\rm H\,I}\,{\rm d}X$ is the number of absorbers with column density between $N_{\rm H\,I}$ and $N_{\rm H\,I} + {\rm d}N_{\rm H\,I}$ over an absorption distance interval dX. The analysis in this paper derives $f(N_{\rm H\,I})$ from the statistics of H I emission-line distributions in the local galaxy population in order to predict the effectiveness of present-day galaxies at accounting for the absorption line statistics. The parameter dX assures that $f(N_{\rm H\,I})$ counts the number of absorbers per comoving unit of length, but since ${\rm d}X/{\rm d}z = 1$ at $z = 0$, we can replace dX with dz in our calculation of $f(N_{\rm H\,I})$. The local $f(N_{\rm H\,I})$ can now be calculated from

$$f(N_{\rm H\,I}) = \frac{c}{H_0}\frac{\sum_i \Phi(\boldsymbol{x}_i) w(\boldsymbol{x}_i) A_i(\log N_{\rm H\,I})}{N_{\rm H\,I}\ \ln 10\ \Delta \log N_{\rm H\,I}}. \tag{2}$$

Here, $\Phi(\boldsymbol{x}_i)$ is the space density of objects with property $\boldsymbol{x}_i$ equal to that of galaxy *i*. In reality, the parameter $\boldsymbol{x}$ could be the H I mass or the optical luminosity of the galaxies in the sample, so that $\Phi(\boldsymbol{x})$ is the H I mass function or the optical luminosity function of galaxies in the local universe. $A_i(\log N_{\rm H\,I})$ is the area function that describes for galaxy *i* the area in Mpc^2 corresponding to a column density in the range $\log N_{\rm H\,I}$ to $\log N_{\rm H\,I} + \Delta \log N_{\rm H\,I}$. In practice, this is simply calculated by summing for each galaxy the number of pixels in a certain $\log N_{\rm H\,I}$ range multiplied by the physical area of a pixel. The function $w(\boldsymbol{x}_i)$ is a weighting function that takes into account the varying number of galaxies across the full stretch of $\boldsymbol{x}$, and is calculated by taking the reciprocal of the number of galaxies in the range $\log \boldsymbol{x} - \Delta/2$ to $\log \boldsymbol{x} + \Delta/2$, where Δ is taken to be 0.3. The results are very insensitive to the exact value of Δ. The summation sign denotes a summation over all galaxies in the sample. Finally, c/H_0 converts the number of systems per Mpc to that per unit redshift. Note that dependencies on H_0 disappear in the final evaluation of $f(N_{\rm H\,I})$.

The WHISP sample that is used in this analysis is somewhat biased towards early-type galaxies (S0 to Sb) because these were specifically targeted for the projects described in van der Hulst et al. (2001). If we were to apply a simple weighting scheme using a luminosity or H I mass function, early-type galaxies would be given too much weight in the calculation of the $f(N_{\rm H\,I})$. To avoid this problem, we choose to apply type-specific H I mass functions as published by Zwaan et al. (2003). Morphological types are available in the Lyon-Meudon Extragalactic Database (LEDA) for all but 18 galaxies in the WHISP sample. We divide the WHISP sample into five subsets of galaxies: E–S0, Sa–Sb, Sbc–Sc, Scd–Sd and Sm–Irr. Visual inspection of the unclassified galaxies learned that these were mostly dwarf irregular or small compact galaxies, and hence we put these in the Sm/Irr subset. We note that the difference between the $f(N_{\rm H\,I})$ calculated using the weights based on one H I mass function for all WHISP galaxies and that based on type-specific weighting is very small.

Fig. 3 shows our measured column density distribution function $f(N_{\rm H\,I})$. We use a binning of $\log N_{\rm H\,I} = 0.1$ dex. The error bars indicate 1σ uncertainties and include uncertainties in the H I mass function normalization from Zwaan et al. (2003) as well as counting statistics of the WHISP sample. The open symbols indicate column densities below $\log N_{\rm H\,I} = 19.8$, which we adopt as our sensitivity limit (see Section 4.1 for a discussion on this limit). Following Pei & Fall (1995), Storrie-Lombardi, Irwin & McMahon (1996), Storrie-Lombardi & Wolfe (2000) and Péroux et al. (2003), we fit $f(N_{\rm H\,I})$ with a gamma distribution, analogous to the Schechter function, which is used for fitting luminosity functions and H I mass functions:

$$f(N_{\rm H\,I}) = (f^*/N^*_{\rm H\,I})(N_{\rm H\,I}/N^*_{\rm H\,I})^{-\beta}{\rm e}^{-N_{\rm H\,I}/N^*_{\rm H\,I}}. \tag{3}$$

This gives an excellent fit to our data with parameters: $\beta = 1.24$, $\log N^*_{\rm H\,I} = 21.2\ {\rm cm}^{-2}$ and $f^* = 0.0193$ if we use all data points above $\log N_{\rm H\,I} > 19.8$. The parametric $f(N_{\rm H\,I})$ is shown as a solid line in

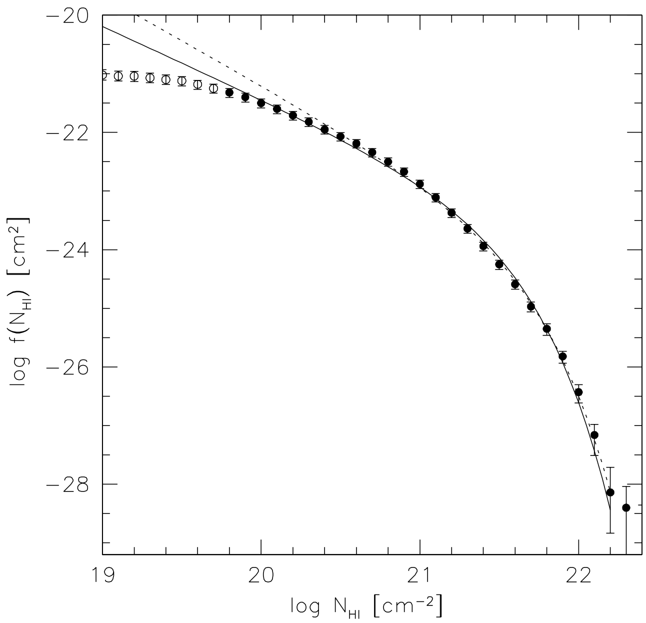

Figure 3. The H I column density distribution function at $z = 0$ from 21-cm emission-line observations. Error bars include uncertainties in the H I mass function as well as counting statistics and indicate 1σ uncertainties. Open symbols correspond to measurements below our sensitivity limit. The solid line is a gamma distribution fit (see equation 3) to all points above $\log N_{\rm H\,I} > 19.8$, the dotted line is the same but restricted to $\log N_{\rm H\,I} > 20.3$.

Fig. 3. If we restrict the fit to column densities above the DLA limit, we find $\beta = 1.52$, $\log N^*_{\rm H\,I} = 21.3\,{\rm cm}^{-2}$ and $f^* = 0.0137$, which is shown by the dotted line. We note that there is no physical motivation for fitting the $f(N_{\rm H\,I})$ with a gamma distribution other than that it provides a reasonable fit. There is also not a physical reason to fit $f(N_{\rm H\,I})$ with a power law, which is traditionally done (e.g. Tytler 1987). However, the good gamma distribution fit demonstrates that at high H I column densities ($\log N_{\rm H\,I} > 21$), the $f(N_{\rm H\,I})$ deviates strongly from a traditional single power-law fit. This is consistent with the form of the cut-off identified by Péroux et al. (2003) based on a large sample of DLAs and sub-DLAs.

The total H I mass density can be calculated by integrating over the column density distribution function. When using the parametrized gamma distribution, it can be easily seen that the H I mass density can be calculated as

$$\rho_{\rm H\,I} = \Gamma(2-\beta) f^* N^*_{\rm H\,I}\, m_{\rm H}\, H_0/c,$$

where $m_{\rm H}$ is the mass of the hydrogen atom and Γ is the Euler gamma function. Using the best-fit parameters of our gamma distribution fit to $\log N_{\rm H\,I} > 19.8$, we find $\rho_{\rm H\,I} = 6.8 \times 10^7\,{\rm M}_\odot\,{\rm Mpc}^{-3}$ in excellent agreement with Zwaan et al. (2003). This may not come as a surprise since we used the H I mass functions from that paper to calibrate $f(N_{\rm H\,I})$. None the less, the result of this calculation is a good consistency check and assures that the normalization of our $f(N_{\rm H\,I})$ is correct (see also Rao & Briggs 1993).

There are a few interesting features in Fig. 3. First, our measured points begin to deviate from the power-law end of the gamma distribution fit at column densities $\log N_{\rm H\,I} < 19.8$. The first obvious explanation for this is that in this range of $N_{\rm H\,I}$ we start to loose sensitivity in the 21-cm maps. There might also be a more physical origin of this effect, which is the expected ionization of the outer H I discs of galaxies by the metagalactic UV background below $\log N_{\rm H\,I} \approx 19.5$ (Corbelli & Salpeter 1993; Maloney 1993). Corbelli & Bandiera (2002) argue that if $f(N_{\rm H\,I})$ is corrected to include H II, it would follow a power law down to $N_{\rm H\,I} = 10^{17}\,{\rm cm}^{-2}$. Our 21-cm maps lack the sensitivity to study this effect in detail. At the high $N_{\rm H\,I}$ end in Fig. 3, the $f(N_{\rm H\,I})$ drops off exponentially, which is faster than $N_{\rm H\,I}^{-3}$ above $\log N_{\rm H\,I} = 21.6$. A fall-off of $N_{\rm H\,I}^{-3}$ is theoretically expected for randomly oriented gas disc, irrespective of their radial $N_{\rm H\,I}$ distribution (see Milgrom 1988; Fall & Pei 1993; Zwaan, Verheijen & Briggs 1999). Three independent effects can cause deviation of the $N_{\rm H\,I}^{-3}$ expectation: (i) beam smearing in the 21-cm maps can smooth out the very highest column densities; (ii) galaxies are not infinitely thin [this is assumed in the $f(N_{\rm H\,I})$ calculation of randomly oriented discs] and (iii) the H I gas is not optically thin at the highest column densities. In the remainder of this paper, our possible biases at the extreme edges of $f(N_{\rm H\,I})$ are not important because we only compare our data with the absorption line data in the intermediate $N_{\rm H\,I}$ range. Furthermore, the cosmological H I mass density is also dominated by the intermediate $N_{\rm H\,I}$ values, as will become clear in Section 5.

4.1 The effect of spatial resolution on $f(N_{\rm H\,I})$

One concern when comparing column densities measured from 21-cm maps with those measured from absorption line systems is the large difference in spatial resolution. The median distance of the WHISP sample is 20 Mpc, implying that for the highest resolution maps the synthesized beam corresponds to ≈1.3 kpc. This is almost 10^5 times greater than the diameter of the optical emission region of a QSO (⩽0.03 pc, e.g. Wyithe, Agol & Fluke 2002), the area probed by DLA column density measurements.

Despite this disparity in resolution, 21-cm emission and Lyα absorption measurements generally seem to be in agreement. Dickey & Lockman (1990) noted a consistency between Lyα absorption measurements towards high latitude stars and 21-cm emission measurement in the Galaxy. There is only one example where a column density from both 21-cm emission and DLA absorption has been measured of the same source. The DLA galaxy SBS 1543+593 has Lyα absorption measured at $2.2 \times 10^{20}\,{\rm cm}^{-2}$ (Bowen et al. 2001), whereas the 21-cm emission at the position of the background QSO is measured to be $5 \times 10^{20}\,{\rm cm}^{-2}$ (Chengalur & Kanekar 2002).

An alternative method to test the effect of resolution is to spatially smooth high-resolution 21-cm maps and measure the resulting column densities and $f(N_{\rm H\,I})$. Ryan-Weber, Staveley-Smith & Webster (2005b) used a high-resolution 21-cm data cube of the Large Magellanic Cloud, and convolved it with circular two-dimensional Gaussians of various widths in the spatial plane. The $N_{\rm H\,I}$ distribution was then re-measured and $f(N_{\rm H\,I})$ was recalculated, based on the new, low-resolution column densities. Lowering the resolution was found to have a truncating effect on the $N_{\rm H\,I}$ distribution, generally decreasing the occurrence of the highest column densities.

For our set of WSRT maps, we can test the effect of lowering the spatial resolution. This is shown in Fig. 4, where we present the $f(N_{\rm H\,I})$ distribution derived from the 30- and 60-arcsec maps, along with that from the original resolution maps. It can be seen that going to lower resolution, the highest column densities are smoothed away, and this flux appears again as lower column densities. Effectively, this causes a 'tilt' of $f(N_{\rm H\,I})$. From this sample, it is impossible to estimate if this tilting would continue if even higher resolution maps would be used. However, for our comparison with DLA data the effect of resolution is probably unimportant because the effects are minimal in the intermediate $N_{\rm H\,I}$ range where we make the comparison.

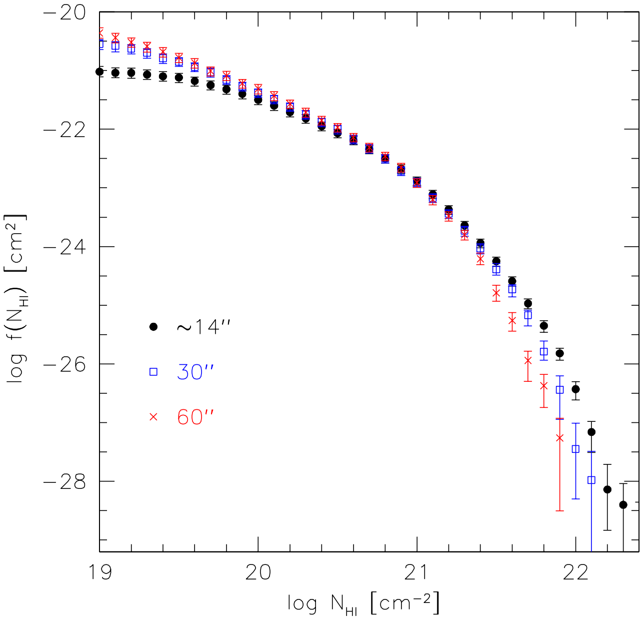

Figure 4. The effect of spatial resolution of the 21-cm line observations on the H I column density distribution function at $z = 0$. Filled circles correspond to the highest resolution, which is approximately 14 arcsec, open squares and crosses are for the spatially smoothed data, to resolutions of 30 and 60 arcsec, respectively.

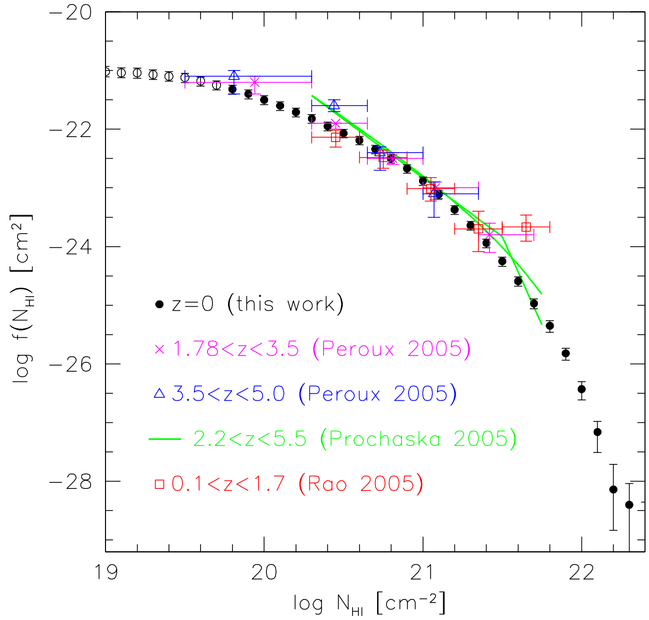

Figure 5. Comparison between the H I column density distribution function at $z = 0$ and higher redshifts. The solid points are from our 21-cm emission-line observations and are the same as in Fig. 3. The higher redshift points are from Péroux et al. (2005) and Rao et al. (2005). Horizontal error bars indicate the bin sizes. The curves show the gamma distribution and double power-law fits to the SDSS-DR3 results from Prochaska et al. (2005) and cover a redshift range of $2.2 < z < 5.5$. All results are based on $\Omega_{\rm m} = 0.3$ and $\Omega_\Lambda = 0.7$ cosmology.

The redshift number density, dN/dz (see Section 6), is also only minimally affected by resolution. The Large Magellanic Cloud study by Ryan-Weber et al. (2005b) showed that dN/dz (at a limit of $\log N_{\rm H\,I} = 20.3$) increases on the order of 10 per cent when the spatial resolution is changed from 15 pc to 1.3 kpc, the typical resolution of the WHISP sample. A 10 per cent change in the measured dN/dz for the WHISP sample is well within the errors quoted in Section 6.

Finally, we comment on our adopted sensitivity limit of $\log N_{\rm H\,I} = 19.8$ for the column density distribution function. In Section 2, we quoted a formal 3σ sensitivity limit of $\log N_{\rm H\,I} = 20.3$ for the high resolution maps, which implies that below this limit we might start to underestimate $f(N_{\rm H\,I})$. However, Fig. 4 shows that $f(N_{\rm H\,I})$ based on lower resolution data is marginally higher in the range $19.8 < \log N_{\rm H\,I} < 20.3$, and only significantly deviates from the high-resolution curve for $\log N_{\rm H\,I} < 19.8$. As explained above, the higher $f(N_{\rm H\,I})$ values for lower resolution data are not only the result of these data having lower sensitivity limits and thus picking up lower column density H I, but also because small regions of high $N_{\rm H\,I}$ gas are smoothed away and appear again as lower column densities. This also explains why small differences between $f(N_{\rm H\,I})$ based on the different resolution data already become apparent above $\log N_{\rm H\,I} = 20.3$. Therefore, if we were to construct a 'hybrid' $f(N_{\rm H\,I})$ using high $N_{\rm H\,I}$ results from high-resolution data and low $N_{\rm H\,I}$ from low-resolution data, we would double-count some of the H I atoms. We choose to simply adopt a sensitivity limit of $\log N_{\rm H\,I} = 19.8$, and note that the low end ($\log N_{\rm H\,I} < 20.3$) of $f(N_{\rm H\,I})$ might be slightly underestimated, but by not more than 20 per cent. This does not influence any of our conclusions presented in this paper.

5 COMPARISON OF $f(N_{\rm H\,I})$ WITH HIGH z DATA

In Fig. 5, we reproduce the $f(N_{\rm H\,I})$ measurements from our analysis of 21-cm maps and compare these with data at higher redshifts from Péroux et al. (2005), Rao, Turnshek & Nestor (2005) and Prochaska et al. (2005). The Péroux et al. (2005) measurements of $f(N_{\rm H\,I})$ below the DLA limit are the result of their new UVES survey for 'sub-DLAs'. We choose here to only plot the points for $\log N_{\rm H\,I} > 19.8$, which roughly corresponds to our sensitivity cut-off. Their higher column density points stem from the combined data of Storrie-Lombardi et al. (1996), Storrie-Lombardi & Wolfe (2000) and Péroux et al. (2001), together based on ≈100 $z > 4$ quasars. The Prochaska et al. (2005) data are from an automatic search for $z > 2.2$ DLAs in the Sloan Digital Sky Survey (SDSS) Data Release 3 (DR3) and also include the results from previous DLA surveys. We represent their results by both a gamma distribution fit and a double power-law fit to the whole data set in the redshift range $2.2 < z < 5.5$. The intermediate redshift points from Rao et al. (2005) are based on Mg II-selected DLAs. All calculations are based on a $\Omega_{\rm m} = 0.3$, $\Omega_\Lambda = 0.7$ cosmology. The surprising result from this figure is that there appears to be only *very mild evolution in the intersection cross-section of H I from redshift* $z \sim 5$ *to the present*. This is a conclusion in stark contrast to earlier works that claimed strong evolution in the DLA cross-section (e.g. Wolfe et al. 1986; Lanzetta et al. 1991). We will come back to this weak evolution in Section 6 in which we discuss the redshift number density.

In Fig. 6, we plot the contribution of systems with different column densities to the integral H I mass density $\rho_{\rm H\,I}$. At $z = 0$, it is clear that systems with column densities $N_{\rm H\,I} \sim 10^{21}$ cm^{-2} dominate the H I mass density. At higher redshifts ($z > 1.7$), the uncertainties are much larger, but also there it appears that $N_{\rm H\,I} \sim 10^{21}$ cm^{-2} systems contribute most, although the Prochaska et al. (2005) data suggest that column densities between $\log N_{\rm H\,I} = 20.3$ and 21.3 contribute almost evenly. Any possible differences between the results at various redshifts are much more pronounced in Fig. 6 than in Fig. 5 because the vertical scale is stretched from nine decades to only four

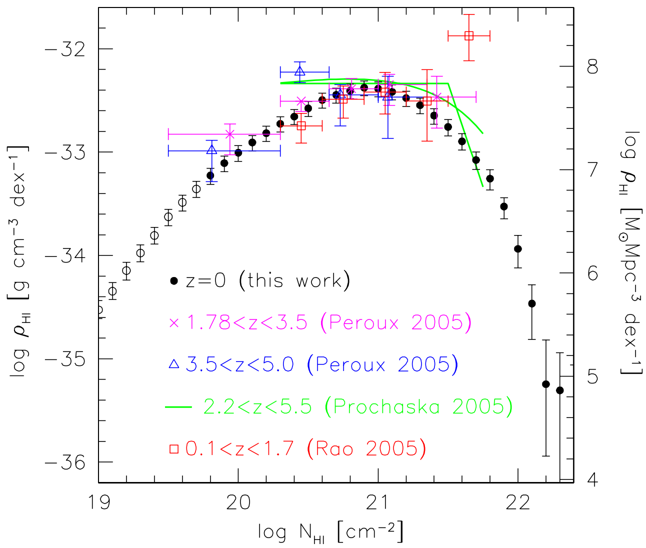

Figure 6. The H I mass density contained in systems of different column density per decade of $N_{\rm HI}$. Solid circles are for $z = 0$ and are from our data, other symbols are for higher redshifts and are derived from Péroux et al. (2005) and Rao et al. (2005). The curves are the converted fits to the SDDS-DR3 results from Prochaska et al. (2005).

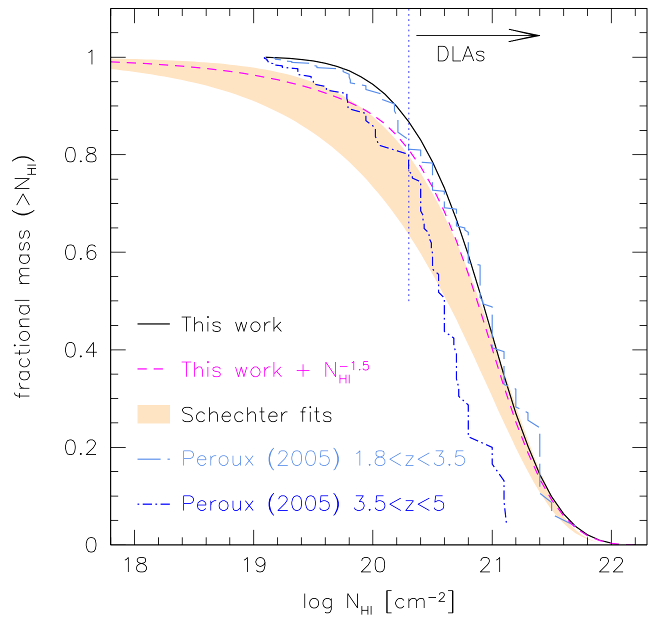

Figure 7. Cumulative H I mass distribution in systems with column density $>N_{\rm HI}$. The solid line is based on our data alone, the dashed line includes a correction for H I gas with column densities below our sensitivity limit and indicates that ≈81 per cent of the integral mass in H I is in classical damped systems with log $N_{\rm HI}$ > 20.3 cm^{-2}. The shaded area indicates the distribution based on the gamma distribution fits to our $f(N_{\rm HI})$ (Fig. 3), where the lower boundary corresponds to the fit to log $N_{\rm HI}$ > 20.3 and the upper boundary to the fit to log $N_{\rm HI}$ > 19.8. The long-dashed and dash-dotted lines are from Péroux et al. (2005) and are for redshift ranges 1.8 < z < 3.5 and z > 3.5, respectively.

decades. The one point that clearly deviates is the highest $N_{\rm HI}$ point from Rao et al. (2005) at log $N_{\rm HI}$ = 21.65. This elevated interception rate of high $N_{\rm HI}$ Mg II-selected intermediate redshift DLAs is present in both redshift bins that Rao et al. (2005) distinguish (0.1 < z < 0.9 and 0.9 < z < 1.7), and is also reported in their earlier work (Rao & Turnshek 2000). Fig. 6 very clearly demonstrates that this point dominates the $\Omega_{\rm HI}$ measurement at intermediate redshifts. It is therefore important to understand whether the Mg II-based results really indicate that high column densities (log $N_{\rm HI}$ ∼ 21.65) are rare at high redshift, then indeed become more abundant at intermediate redshifts (0.1 < z < 1.7) and subsequently evolve to the scarce numbers at z = 0. Alternatively, the high $f(N_{\rm HI})$ point might be a result of yet unidentified selection effects introduced by the Mg II selection, although presently there are no indications that support this (Péroux et al. 2004; Rao et al. 2005).

To further investigate the relative contribution of different column densities to the H I mass density, we plot in Fig. 7 the cumulative H I mass density as a function of column density. The solid curve is based on our measured $f(N_{\rm HI})$ points, not on the gamma distribution fit to the data. From this curve alone, we would conclude that at z = 0 the fractional mass in systems with log $N_{\rm HI}$ > 20.3 (classical DLAs) is 86 per cent. However, the contribution of gas with column densities below our sensitivity limit of approximately log $N_{\rm HI}$ = 19.8 is very uncertain. Unfortunately, only selective regions have been imaged to low column density limits, but no large-scale 21-cm emission-line surveys that reach sensitivities below log $N_{\rm HI}$ = 19.8 are available yet. For example, the M31 environment has been imaged with the Green Bank Telescope and the WSRT at resolutions between 50 pc and 11 kpc (Braun & Thilker 2004, and references therein), covering the column density range 17 < log $N_{\rm HI}$ < 22. However, the H I emission in this region is mostly due to discrete high-velocity clouds (HVCs) physically associated to M31. These surveys may not be representative of all low column density H I gas at z = 0, and do not provide good constraints on the shape of $f(N_{\rm HI})$. To obtain a rough estimate of the contribution of gas below our sensitivity limit, we extrapolate our measured $f(N_{\rm HI})$ below log $N_{\rm HI}$ = 19.8 with $f(N_{\rm HI}) \propto N_{\rm HI}^{-1.5}$ (per e.g. Tytler 1987) and find that the fractional mass in systems with log $N_{\rm HI}$ > 20.3 is ≈81 per cent, and hence only ≈19 per cent of the H I atoms in the local universe are in sub-DLA column densities. For illustrative purposes, we also show as a shaded area the cumulative distribution functions based on the gamma distribution fits to $f(N_{\rm HI})$ as presented in Fig. 3. Here, the fit to log $N_{\rm HI}$ > 19.8 corresponds to the upper boundary and the fit to log $N_{\rm HI}$ > 20.3 to the lower boundary to this area. Obviously, simply extrapolating the gamma distribution fits to $f(N_{\rm HI})$ below the DLA limit results in a severe overestimation of the number of H I atoms in sub-DLAs.

The higher redshift curves are based on the data of Péroux et al. (2005). With their new column density measurements of individual sub-DLAs, these authors improved the earlier estimates of $f(N_{\rm HI})$ presented in Péroux et al. (2003) and now show that the fractional contribution of sub-DLAs to $\Omega_{\rm HI}$ is approximately 20 per cent at all redshifts z > 1.8. These curves also indicate that at high redshifts the highest column densities are relatively rarer, as can also be seen in Fig. 5. Prochaska et al. (2005) estimate the fractional contribution of sub-DLAs to the integral mass density by combining their measured $f(N_{\rm HI})$ with the redshift number density of sub-DLAs from Péroux et al. (2001). They conclude that the sub-DLAs (or super-LLSs in their terminology) contribute between 20 and 50 per cent over the redshift range 2.2–5.5, but emphasize that their single power-law fit to $f(N_{\rm HI})$ might even underestimate this fraction. Obviously, the importance of sub-DLAs at high redshift remains a topic needing further clarification in the future.

The fact that from our high-resolution 21-cm maps we find that ≈81 per cent of the H I mass density at z = 0 is in column densities above the DLA limit implies that $\Omega_{\rm H\,I}$ measurements from blind 21-cm surveys overestimate $\Omega_{\rm DLA}$ ($z = 0$) by only ≈23 per cent. When comparing measurements of the atomic gas mass density at high and low z, it is important that the $z = 0$ value be corrected with a factor of 0.81 when compared to measurements from DLAs. On the other hand, when at higher redshift the sub-DLA contribution is taken into account (e.g. Péroux et al. 2005), no correction of the $z =$ 0 value is required. We refer to Prochaska et al. (2005) for various definitions of $\Omega_{\rm gas}$ and their recommended usage.

6 THE REDSHIFT NUMBER DENSITY AT $z = 0$

The redshift number density dN/dz for column densities larger than $N_{\rm H\,I}$ can be calculated from the $z = 0$ $f(N_{\rm H\,I})$ distribution by summing over all column densities larger than $N_{\rm H\,I}$:

$$\mathrm{d}N/\mathrm{d}z = \int_{N'_{\rm H\,I}>N_{\rm H\,I}} f(N'_{\rm H\,I})\,\mathrm{d}N'_{\rm H\,I} \quad (4)$$

$$= \frac{c}{H_0} \sum_{N'_{\rm H\,I}>N_{\rm H\,I}} \frac{\sum_i \Phi(\boldsymbol{x}_i) w(\boldsymbol{x}_i) A_i(\log N'_{\rm H\,I})}{\Delta \log N'_{\rm H\,I}}, \quad (5)$$

where definitions of Φ, w and A_i are equal to those in Section 4. In Fig. 8, we show dN/dz as a function of $N_{\rm H\,I}$. For column densities in excess of the DLA limit of $\log N_{\rm H\,I} = 20.3$, we find dN/dz = 0.045 ± 0.006, where the 1σ uncertainty is dominated by the uncertainty in the parameters of the H I mass function that is used to calibrate $f(N_{\rm H\,I})$. For larger column densities, dN/dz drops rapidly, systems with $\log N_{\rm H\,I} > 21$ contribute only 20 per cent to the total DLA cross-section. Our measurement of dN/dz translates into a mean cross-section density of $\langle n\sigma \rangle = (1.13 \pm 0.15) \times 10^{-5}\,{\rm Mpc}^{-1}$, or to a mean free path between absorbers of $l = \langle n\sigma \rangle^{-1} = 88 \pm 12$ Gpc.

The value of dN/dz ($z = 0$) = 0.045 agrees very well with our previous measurement of dN/dz = 0.042 ± 0.015, based on a much smaller sample of galaxies (Zwaan et al. 2002). Rosenberg & Schneider (2003) used H I-selected galaxies to find dN/dz = 0.053 ± 0.013, also in good agreement with our value. Their slightly higher value is probably the result of the steeper H I mass function slope that these authors use to calibrate their $f(N_{\rm H\,I})$. Ryan-Weber et al. (2003) also used a sample of H I-selected galaxies observed with the ATCA and applied the same H I mass function (HIMF) normalization as in the present analysis to find dN/dz = $0.046^{+0.03}_{-0.02}$ (see also Ryan-Weber et al. 2005a). An earlier calculation by Rao & Briggs (1993) resulted in a much lower value of dN/dz = 0.015. This discrepancy arises partly because these authors limited their analysis to large, optically bright galaxies, whereas the newer values take into account dwarf and LSB galaxies, and partly because their calculation is based on the Gaussian luminosity function from Tammann (1985), which has a lower normalization than the most recent H I mass function measurements.

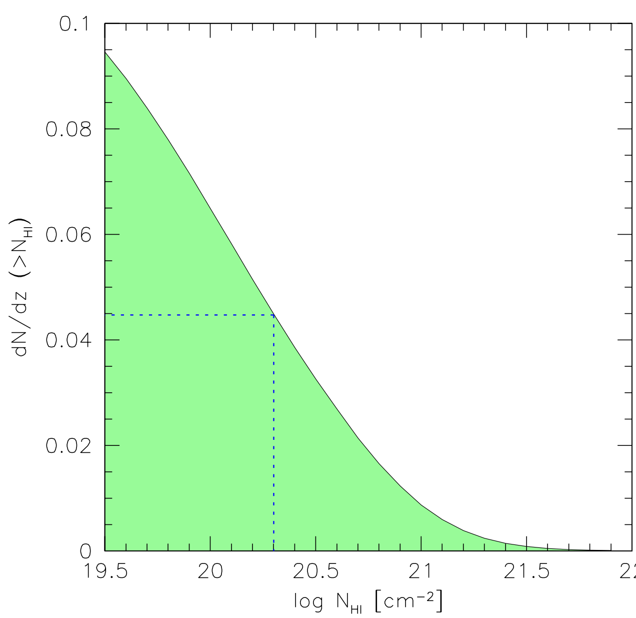

Figure 8. Integral redshift number density dN/dz as a function of H I column density cut-off. For $\log N_{\rm H\,I} > 20.3\,{\rm cm}^{-2}$, we find d$N$/d$z$ = 0.045 dropping rapidly for higher column densities.

It has been noted before that the area of the H I disc of galaxies above the DLA limit correlates very tightly to the H I mass (e.g. Broeils 1992; Rosenberg & Schneider 2003). We can make use of this correlation to obtain an alternative measurement of dN/dz. Suppose that the projected H I area A correlates with $M_{\rm H\,I}$ as $A \propto \beta M_{\rm H\,I}$, and A^* is the projected area of an $M^*_{\rm H\,I}$ galaxy, then

$$\mathrm{d}N/\mathrm{d}z = \frac{c}{H_0} \int \theta(M_{\rm H\,I}) A(M_{\rm H\,I})\,\mathrm{d}M_{\rm H\,I} \quad (6)$$

$$= \frac{c}{H_0} A^* \theta^* \Gamma(1 + \alpha + \beta), \quad (7)$$

where θ^* and α are the normalization and the low-mass power-law slope of the H I mass function, respectively. For our WHISP sample, we find that $A^* = 992\,{\rm kpc}^2$. Using this value, the Zwaan et al. (2003) H I mass function parameters ($\alpha = -1.30$ and $\theta^* = 0.0086\,{\rm Mpc}^{-3}$), and $\beta = 1$, we find that dN/dz = 0.044. Quite surprisingly, this simplistic approach yields a result very close to our measurement of dN/dz = 0.045 based on a much more detailed analysis.

6.1 Evolution of d*N*/d*z*

We now have a robust measurement of the redshift number density at $z = 0$. How does this value compare to DLA measurements at higher redshifts? In Fig. 9, we show the combined results of high- and low-z dN/dz measurements from different surveys. At $z = 0$, we plot our points as well as those from Ryan-Weber et al. (2003, 2005a) and Rosenberg & Schneider (2003). All these local values are based on the analyses of H I 21-cm maps of galaxies, have small error bars and are consistent with each other. The points at $z \approx$ 0.6 and ≈1.2 are from Rao et al. (2005) based on their $z < 1.65$ *HST* survey of Mg II selected systems from the SDSS Early Data Release. Their total sample of $z < 1.65$ DLAs is now 41, which is a considerable improvement over the original sample of 16 DLAs presented in Rao & Turnshek (2000). The underlying assumption that the incidence of DLAs can be derived from Mg II surveys relies on the empirical fact that all DLAs show Mg II absorption, whereas the reverse is not true. The known incidence of Mg II systems can therefore be used to bootstrap the DLA statistics. A similar technique was used by Churchill (2001), who found dN/dz = $0.08^{+0.09}_{-0.05}$ at a median redshift of $z = 0.05$. This number is based on *HST* data on four Mg II absorbers. The high redshift points from Prochaska et al. (2005) are the result of an automatic search for $z > 2.2$ DLAs in SDSS-DR3 and also include the results from previous DLA surveys as summarized in Storrie-Lombardi & Wolfe (2000) and Péroux et al. (2003).

Also shown in Fig. 9 by a dashed line is the fit dN/dz = $0.055\,(1 + z)^{1.11}$ from Storrie-Lombardi & Wolfe (2000), which agrees reasonably well with the $z = 0$ value. It is often quoted in the literature that

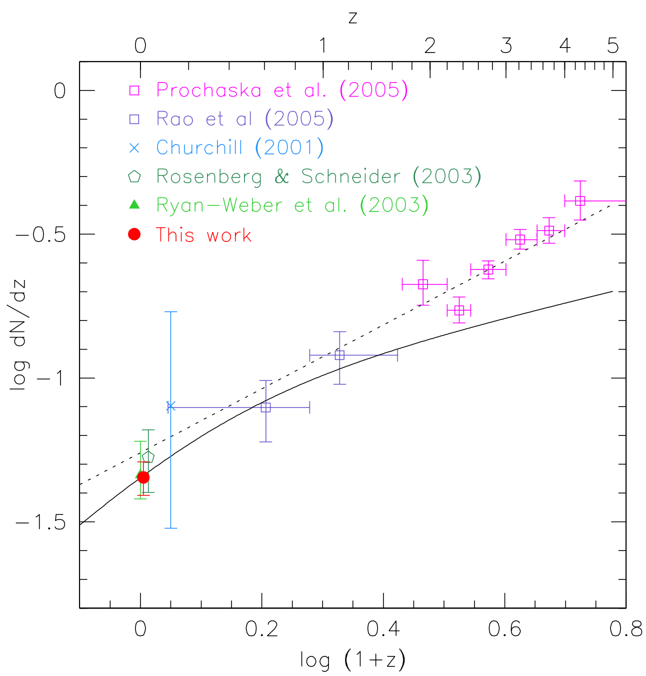

Figure 9. Number density of DLAs per unit redshift as function of redshift. All points at $z > 0.1$ are from UV and optical surveys for DLAs or Mg II systems (see text). The points at $z \sim 0$ are from techniques similar to that presented in this work. The dashed line shows the best fit to $\mathrm{d}N/\mathrm{d}z$ from Storrie-Lombardi & Wolfe (2000). The solid line represents 'no evolution in the product of cross-section and comoving space density' for a cosmology with $\Omega_{\mathrm{m}} = 0.3$ and $\Omega_\Lambda = 0.7$. This line is scaled vertically so as to fit our $z = 0$ point.

this fit indicates 'no intrinsic evolution in the product of space density and cross-section' of damped absorbers, which is another way of saying that the number of systems per comoving unit of length does not evolve. This statement is based on the fact that for a $q_0 = 0$ universe, $\mathrm{d}X/\mathrm{d}z = 1 + z \approx (1 + z)^{1.11}$. However, for a modern non-zero Λ universe, $\mathrm{d}X/\mathrm{d}z$ is given by

$$\frac{\mathrm{d}X}{\mathrm{d}z} = \frac{(1+z)^2}{\sqrt{\Omega_{\mathrm{M}}(1+z)^3 - (\Omega_{\mathrm{M}} + \Omega_\Lambda - 1)(1+z)^2 + \Omega_\Lambda}}, \quad (8)$$

which starts to deviate significantly from the $q_0 = 0$ prediction for $z > 1$. For no evolution in the number of systems per comoving unit of length, we expect

$$\frac{\mathrm{d}N}{\mathrm{d}z} = \left(\frac{\mathrm{d}N}{\mathrm{d}z}\right)_{z=0} \frac{\mathrm{d}X}{\mathrm{d}z}. \quad (9)$$

The solid line in Fig. 9 represents this run of $\mathrm{d}N/\mathrm{d}z$ as a function of z for an $\Omega_{\mathrm{m}} = 0.3$ and $\Omega_\Lambda = 0.7$ universe. We normalize this line to our $\mathrm{d}N/\mathrm{d}z(z = 0) = 0.045$ measurement. With respect to this $\Omega_{\mathrm{m}} = 0.3$, $\Omega_\Lambda = 0.7$ prediction, there is only weak evolution in the comoving incidence rate from $z \sim 4$ to the present time. Between $z \sim 1.5$ and 0, there is no evidence for evolution at all, between $z \sim 4$ and 0, the evolution in the comoving incidence rate is approximately a factor of 2.

This conclusion contrasts with previous claims that the local galaxy population cannot explain the DLA incidence rate. For example, estimates of the cross-section to DLA absorption in local galaxy discs by Wolfe et al. (1986) and Lanzetta et al. (1991) indicated that there should be evolution of at least a factor of 2–4 (depending on the value of q_0). Similarly, the analysis of Rao & Briggs (1993) pointed towards strong evolution in the incidence rate since $z = 2.5$. Part of the reason for our conclusion being different from older works is the change in cosmological parameters. For no evolution in the comoving number density in a $q_0 = 0.5$ cosmology, the allowed change in $\mathrm{d}N/\mathrm{d}z$ is much smaller than that for a modern $\Omega_{\mathrm{m}} = 0.3$, $\Omega_\Lambda = 0.7$ cosmology. The other reason is that the galaxy luminosity functions that were used for older $\mathrm{d}N/\mathrm{d}z$ calculations had a lower normalization than the more recent estimates from large-scale optical and 21-cm surveys.

We emphasize that the normalization of $f(N_{\mathrm{H\,I}})$ and hence of $\mathrm{d}N/\mathrm{d}z$ is completely independent of the WHISP galaxy sample, but instead depends only on the H I mass functions derived from HIPASS. This is a large-scale blind 21-cm emission-line survey covering the whole southern hemisphere and the redshift range $z = 0$ to $z = 0.04$. Most of the weight to the normalization of the H I mass function comes from galaxies around $z = 0.01$. Optical and infrared surveys have shown that a large angular area around the southern Galactic pole is underdense by ≈25 per cent extending out to $z = 0.1$ (Frith et al. 2003; Busswell et al. 2004). This area occupies approximately one-third of the HIPASS sky coverage, but it is not clear whether the underdensity extends to even larger regions in the southern hemisphere. In any case, our measured $f(N_{\mathrm{H\,I}})$ and $\mathrm{d}N/\mathrm{d}z$ might be underestimated by up to 25 per cent due to this local galaxy deficiency. This implies that the evolution in the comoving incidence rate is perhaps even slightly weaker than portrayed in Fig. 9.

The lack of evolution in the comoving incidence rate since redshift $z \sim 1.5$ implies that the average H I cross-section above the DLA limit has not changed significantly over half the age of the universe. At present, it is difficult to ascertain whether this should be interpreted as no evolution in the DLA population – meaning no change in the space density *and* size of DLA absorbing systems – or as a combined effect where an evolving space density is compensated by a change in mean absorber size.

7 EXPECTED PROPERTIES OF LOW-Z DLA HOST GALAXIES

In this section, we calculate the probability distribution functions of the expected properties of galaxies responsible for high column density H I absorption at $z = 0$. To this end, we define a quantity $\mathcal{N}$ as the 'volume density of cross-sectional area' for different column density cut-offs. $\mathcal{N}$ is calculated as

$$\mathcal{N}(\boldsymbol{y}) = \int \Sigma(\boldsymbol{y}, \boldsymbol{x})\Phi(\boldsymbol{x})\,\mathrm{d}\boldsymbol{x}, \quad (10)$$

where $\Sigma(\boldsymbol{y}, \boldsymbol{x})$ is the cross-sectional area of H I in Mpc^2 above a certain column density cut-off as a function of galaxy properties $\boldsymbol{x}$ and $\boldsymbol{y}$, and $\Phi(\boldsymbol{x})$ is the space density of galaxies in Mpc^{-3} as a function of $\boldsymbol{x}$. Similar to the calculation of $f(N_{\mathrm{H\,I}})$, the parameter $\boldsymbol{x}$ has elements $M_{\mathrm{H\,I}}$ and L, such that Φ is again the H I mass function or the optical luminosity function that is used to calculate real space densities. The vector $\boldsymbol{y}$ could be any galaxy property, such as optical surface brightness or morphological type. For example, if $\boldsymbol{x} = M_{\mathrm{H\,I}}$ and $\boldsymbol{y} = \mu$, we calculate $\mathcal{N}(\mu)$, the volume density of cross-sectional area as a function of surface brightness μ, using the H I mass function to calculate space densities. In the remainder of this paper, we will use $\boldsymbol{x} = M_{\mathrm{H\,I}}$, so that the H I mass function is used for calibration. We find that the conclusions would not change significantly if we were to use the optical luminosity function instead.

Another way of looking at $\mathcal{N}$ is that it defines the number of systems above a certain column density limit that would be encountered along a random 1-Mpc path through the $z = 0$ Universe. Put

Table 3. Relative contribution to DLA cross-section from different galaxies.

Quantity	$<L_*/10$	$<L_*/5$	$<L_*$	$<2L_*$
L	0.45	0.58	0.87	0.96
$M_{\rm H\,I}$	0.22	0.37	0.81	0.96

Table 4. Expected properties of low-z DLAs.

Quantity	Median	Mean	Logarithmic mean
M_B	$-18.1^{+2.6}_{-1.9}$	-19.2	-17.7
$\log M_{\rm H\,I}$ ($M_\odot$)	$9.3^{+0.5}_{-0.7}$	9.5	9.0
b (kpc)	$7.6^{+10.2}_{-5.0}$	10.6	7.0

differently, $\mathcal{N}$ can be written as $dN/dz \times H_0/c$, where dN/dz, the number of systems per unit redshift, is a familiar quantity in QSO absorption line studies. The run of $\mathcal{N}$ as a function of galaxy property $\boldsymbol{x}$ represents the probability distribution of $\boldsymbol{x}$ of galaxies responsible for absorption above a certain column density.

In the following, we present this probability distribution for four different column density limits, $\log N_{\rm H\,I} > 19.8$, > 20.3, > 20.8 and >21.3. The distribution for $\log N_{\rm H\,I} = 20.3$, which is the classical DLA limit, is always shown as a thick line. In Table 3, we tabulate the relative contributions of galaxies of different luminosities and H I masses to the total DLA cross-section. In Table 4, the mean and median properties of expected DLA host galaxies are summarized.

7.1 Luminosities

In Fig. 10, we show $\mathcal{N}$ as a function of B-band absolute magnitude. As described in the preceding section, this distribution is calculated by multiplying the H I mass function with the cross-sectional area above a certain column density cut-off, and binning in absolute magnitude. The two lower panels in Fig. 10 show the effect of changing the slope of the HIMF that is used to calibrate the distribution. The luminosity measurements are taken from the RC3, or when these are not available, from LEDA, which gives B-band magnitudes transformed to the RC3 system. Since we use the L_* measurement from Norberg et al. (2002), which is in the $b_{\rm J}$ system, we convert our magnitudes to $b_{\rm J}$ using $b_{\rm J} = B_{\rm RC3} + 0.185$ as derived by Liske et al. (2003), and hence Fig. 10 is approximately in the $b_{\rm J}$ system. What is immediately obvious from this plot is that the probability distribution is not strongly peaked around L_* galaxies. Rather, for column densities above the DLA limit, the distribution is almost flat between $M_B \approx -15$ and $M_B \approx -20$. The consequence of this is that if an H I column density $N_{\rm H\,I} > 10^{20.3}$ cm^{-2} is encountered somewhere in the local universe, the probability that this gas is associated with an $L_*/50$ galaxy is only slightly lower than for association with an L_* galaxy. More specifically, 87 per cent of the DLA cross-section is in sub-L_* galaxies and 45 per cent of the cross-section is in galaxies with $L < L_*/10$. These numbers agree very well with the luminosity distribution of $z < 1$ DLA host galaxies. Taking into account the three non-detections of DLA host galaxies and assuming that these are $\ll L_*$, we find that 80 per cent of the $z < 1$ DLA galaxies is sub-L_*. The median absolute magnitude of a $z = 0$ DLA galaxy is expected to be $M_B = -18.1$ ($\sim L_*/7$), with 68 per cent in the range $-15.5 < M_B < -20.0$, whereas the mean luminosity is $L_*/2.5$.

By studying a sample of low-z DLA galaxies, Rao et al. (2003) also conclude that low-luminosity galaxies dominate the H I cross-section, whereas Chen & Lanzetta (2003) claim that luminous galaxies can explain most of the DLAs and that a contribution by dwarfs is not necessary. The origin of this apparent disagreement lies in the definition of a dwarf galaxy. Using the definition of Rao et al. (2003) that all sub-L_* are dwarfs, these galaxies would indeed dominate the DLA cross-section. However, using the more stringent definition of dwarf galaxies being fainter than $L_*/10$, these systems only contribute approximately 45 per cent of the cross-section.

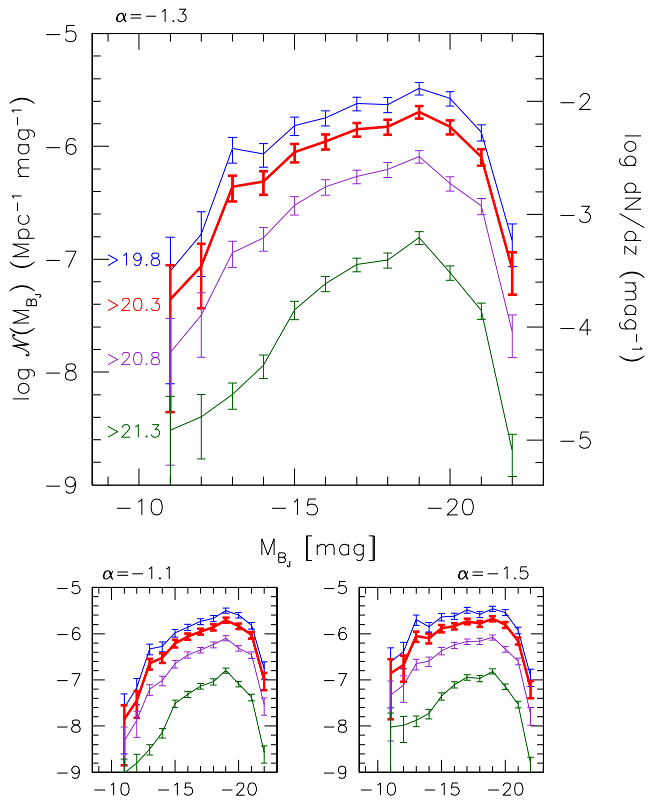

Figure 10. The expected distribution of absolute B-band magnitudes of high column density H I absorbing systems. The lines plus error bars show the product of cross-sectional area and space density, which translates to the number of expected absorbers per Mpc per magnitude. The right axis shows the corresponding number of absorbers per unit redshift dN/dz. The different lines correspond to different column density limits, as indicated by the labels. The thick line corresponds to the classical DLA limit of $\log N_{\rm H\,I} > 20.3$. The smaller panels show the effect of changing the slope of the low-mass slope of the H I mass function that is used to calculate the normalization.

What can also be seen from Fig. 10 is that the highest column densities ($\log N_{\rm H\,I} > 21.3$) are largely associated with the most luminous galaxies: the probability distribution for the highest column densities is more peaked around L_*. Small cross-sections of very high column density gas can still account for high H I masses, which explains why the total H I mass density is dominated by L_* galaxies.

7.2 H I masses

In Fig. 11, we show $\mathcal{N}$ per decade of H I mass as a function of log H I mass. This figure shows largely the same behaviour as Fig. 10, but the distribution is somewhat more peaked around $M^*_{\rm H\,I}$ galaxies ($\log M^*_{\rm H\,I}/M_\odot = 9.8$). The contribution from sub-$M^*_{\rm H\,I}$ galaxies to the total DLA cross-section is still 81 per cent that of galaxies with H I masses lower than $10^9\ M_\odot$ is 31 per cent. These figures agree

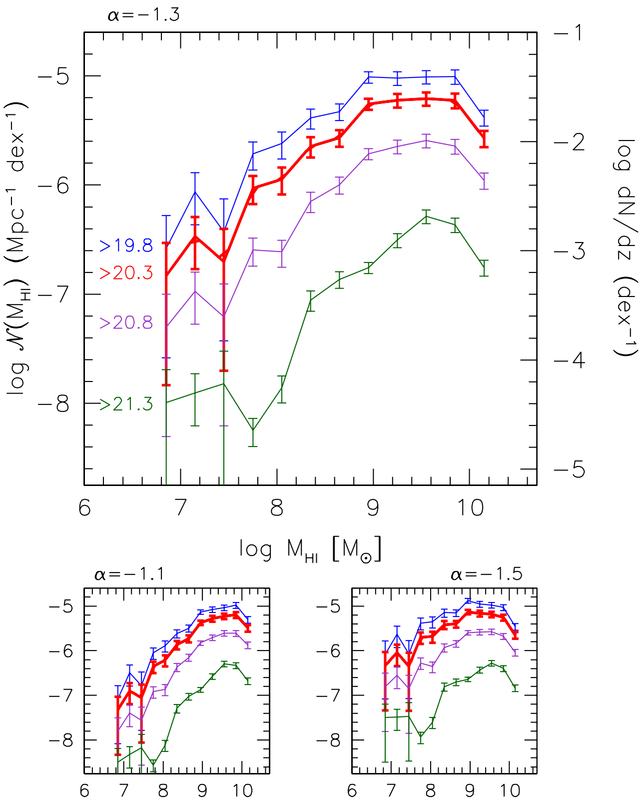

Figure 11. The expected distribution of the H I masses of high column density H I absorbing systems. The lines plus error bars show the product of cross-sectional area and space density, which translates to the number of expected absorbers per Mpc per decade of H I mass. The right axis shows the corresponding number of absorbers per unit redshift dN/dz. The different lines correspond to different column density limits, as indicated by the labels. The thick line corresponds to the classical DLA limit of $\log N_{\rm H\,I} > 20.3$. The smaller panels show the effect of changing the slope of the low-mass slope of the H I mass function that is used to calculate the normalization.

very well with those of Rosenberg & Schneider (2003) and Ryan-Weber et al. (2003) based on samples of galaxies observed with lower spatial resolution. The median H I mass of a $z = 0$ DLA galaxy is expected to be $\log M_{\rm H\,I}/{\rm M}_\odot = 9.3$, with 68 per cent in the range $8.5 < \log M_{\rm H\,I}/{\rm M}_\odot < 9.8$. Again, we see that the highest column densities are preferentially associated with the most massive galaxies. We will come back to this fact in Section 7.5.

7.3 Surface brightness and Hubble type

The probability distribution function of μ_B^{25}, the mean B-band surface brightness within the 25th mag arcsec^{-2}, is given in Fig. 12. Similar to the finding of Ryan-Weber et al. (2003), we find that the cross-section is dominated by galaxies with μ_B^{25} in the range 23–24 mag arcsec^{-2}. For reference, for our sample we find the median value of μ_B^{25} for L_* galaxies is 23.6 mag arcsec^{-2}. At the bright end the distribution drops rapidly, showing that galaxies with high surface brightnesses contain a small fraction of the cross-section. Towards dimmer galaxies, the distribution drops off slowly. We find that 53 per cent of the DLA cross-section is in galaxies dimmer than $\mu_B^{25} = 23.6$ mag arcsec^{-2}. However, for 8 per cent of the galaxies in our sample no measurement of μ_B^{25} is available. Assuming that these galaxies have no measurement because of their LSB, we are biased against LSB galaxies. Including these in our lowest μ_B^{25}

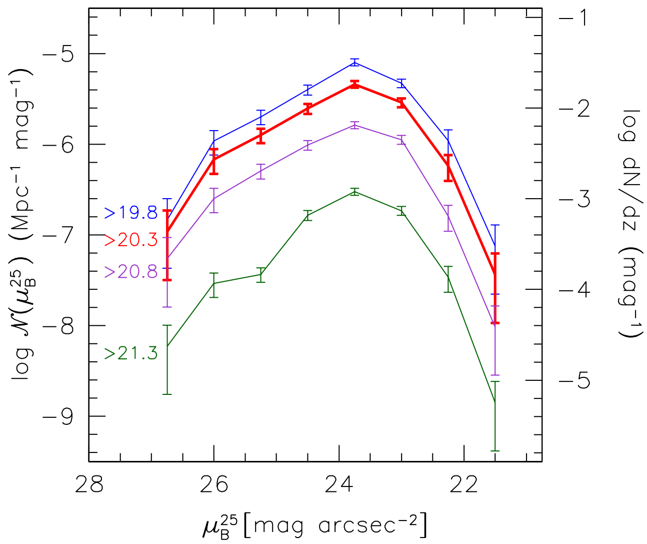

Figure 12. The expected distribution of the B-band surface brightness within the 25th mag isophote of host galaxies of high column density H I absorbing systems. The lines plus error bars show the product of cross-sectional area and space density, which translates to the number of expected absorbers per Mpc per magnitude. The right axis shows the corresponding number of absorbers per unit redshift dN/dz. The different lines correspond to different column density limits, as indicated by the labels. The thick line corresponds to the classical DLA limit of $\log N_{\rm H\,I} > 20.3$.

bins increases the fraction of cross-section in galaxies dimmer than 23.6 mag arcsec^{-2} to 64 per cent.

The measurement of optical surface brightness that we have used tends to understate the contribution of LSB galaxies to the DLA cross-section. The reason for this is that if the surface brightness is measured within a fixed isophote, the radius of this isophote shrinks if the surface brightness decreases. μ_B^{25} is therefore always measured over the central brightest part of a galaxy, which naturally decreases the dynamic range in surface brightness measurements. A better alternative would be $\mu_B^{\rm eff}$, the effective surface brightness (the average surface brightness within the half-light radius), but unfortunately this parameter is only available for 40 per cent of the galaxies in the WHISP sample. For illustrative purposes, we can assign values of $\mu_B^{\rm eff}$ to those galaxies that have no measurements by using the surface brightness–luminosity relation observed for nearby galaxies, for example by Cross & Driver (2002). For galaxies without $\mu_B^{\rm eff}$, we simply take the measurement of the galaxy closest in absolute magnitude in our sample. Thus, we find that the probability distribution of $\mu_B^{\rm eff}$ is much flatter at the LSB end than that of μ_B^{25}. Specifically, we find that 71 per cent of the cross-section is in galaxies dimmer than $\mu_B^{\rm eff} = 22.0$ mag arcsec^{-2}, which corresponds to the peak of the distribution for L_* galaxies. If an LSB galaxy is defined as having a surface brightness fainter than 1.5 mag arcsec^{-2} below this value, we find that 44 per cent of the cross-section is in LSB galaxies, in accordance with the findings of Minchin et al. (2004). The fractional contribution of LSB galaxies to the DLA cross-section is larger than their contribution to the H I mass density because their typical H I mass densities are lower than those observed in high surface brightness galaxies (e.g. de Blok & McGaugh 1997). This is supported by the galaxy formation models of Mo, Mao & White (1998), which indicate that cross-section selected samples are weighted towards galaxies with high angular momentum (i.e. LSB galaxies). In conclusion, our data are not ideal to make firm statements about the contribution of LSB galaxies to the DLA cross-section. However,

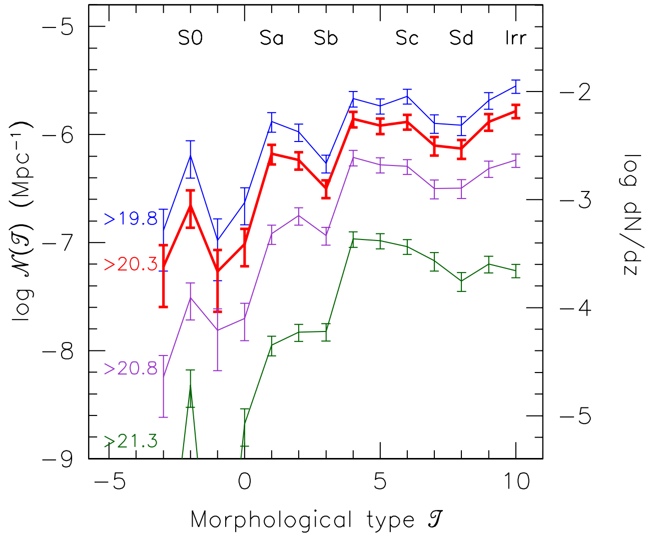

Figure 13. The expected distribution of the morphological types of host galaxies of high column density H I absorbing systems. The lines plus error bars show the product of cross-sectional area and space density, which translates to the number of expected absorbers per Mpc. The right axis shows the corresponding number of absorbers per unit redshift dN/dz. The different lines correspond to different column density limits, as indicated by the labels. The thick line corresponds to the classical DLA limit of $\log N_{\rm H\,I} > 20.3$.

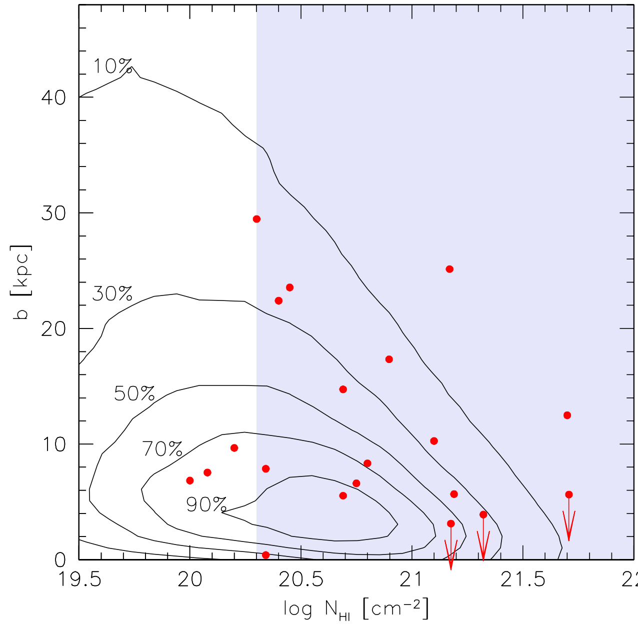

Figure 14. The two-dimensional probability distribution of H I cross-section in the H I column density–impact parameter plane. The contours are calculated from our H I 21-cm maps and are drawn at 10, 30, 50, 70 and 90 per cent of maximum. The points are from DLA galaxy searches in the $z < 1$ universe. The shaded area shows the column density region corresponding to classical damped systems ($\log N_{\rm H\,I} > 20.3$).

using the information we have available we can state that galaxies with surface brightness dimmer than that of a typical L_* galaxy make up at least half of the cross-section.

Turning now to the Hubble types, we see in Fig. 13 that late-type galaxies are preponderant in the distribution of DLA cross-section. Earlier types are not negligible and the probability of identifying an S0 galaxy with a DLA is approximately a third of finding an Sc galaxy.

7.4 Impact parameters

Fig. 14 shows the probability distribution of H I cross-section in the $N_{\rm H\,I}$-b plane, where b is the impact parameter in kpc from the position of the observed column density to the centre of the galaxy. The WHISP sample was used to calculate the cross-sectional area contributed by each element $dN_{\rm H\,I}\, db$ on a fine grid in the $N_{\rm H\,I}$-b plane. We again used the type-specific H I mass functions to assign weights to each individual galaxy (see Section 4). To increase the signal-to-noise ratio in the figure, we smoothed the probability distribution with a Gaussian filter, which results in a final resolution of $\sigma = 0.13$ dex in the $N_{\rm H\,I}$ direction and $\sigma = 1.3$ kpc in the b direction. The contour levels are chosen at 10, 30, 50, 70 and 90 per cent of the maximum value. The shaded area in the figure indicates the column density region that corresponds to DLA column densities.

A few interesting features can be readily seen in Fig. 14. The lowest contour illustrates that the highest H I column densities are very rarely seen at large galactocentric radii: there appears to be a strong correlation between $N_{\rm H\,I}$ and the maximum radius at which this is observed. The observational fact that the H I distribution in galaxies often shows a central depression can be seen by the compression of contours near $b = 0$ kpc. Finally, this plot shows that the largest concentration of H I cross-section in galaxies in the local universe is in column densities in the range $20.3 < \log N_{\rm H\,I} < 20.8$ and impact parameters $b < 7$ kpc.

The points in Fig. 14 are the pairs of $N_{\rm H\,I}$ and b measurements from the literature sample of low-z DLA galaxies from Table 2. If low-z DLAs are drawn from the same population of galaxies as those in our sample from the local universe, we would expect the points to show the same distribution as the contours. Unfortunately, the statistics are too poor to calculate contours from the DLA galaxy data, but there seems to be a qualitative agreement between the two data sets.

A more straightforward comparison between the DLA galaxies and local galaxy properties is presented in Fig. 15, which shows the conditional probability distribution of impact parameter b as a function of column density $N_{\rm H\,I}$. This figure is calculated by normalizing at each value of $N_{\rm H\,I}$ in Fig. 14 the distribution function of cross-section as function of b to the peak of the distribution. The solid line shows the median b value as a function of $N_{\rm H\,I}$, the other lines show the 10th, 25th, 75th, 90th and 99th percentiles, respectively. The literature values are again overplotted as points. Both in the $z = 0$ data and in the DLA data, there is a weak correlation between $N_{\rm H\,I}$ and b. Rao et al. (2003) also noted the existence of this relation. The agreement between the points and the contours is remarkably good: 50 per cent of the literature values are within the 25th and 75th percentiles, and 75 per cent are within the 10th and 90th percentile contours. Based on our analysis, the expected median impact parameter of $\log N_{\rm H\,I} > 20.3$ systems is 7.8 kpc, whereas the median impact parameter of identified $z < 1$ DLA galaxies is 8.3 kpc. Although we are limited by small number statistics, a comparison between the contours and the points suggests that the observed number of very low b systems is lower than expected. These identifications are the ones most likely to be missed due to the proximity of the bright background QSO. Alternatively, if dust obscuration in DLA host galaxies is important, these low b sightlines are expected to be the first to drop out of a flux-limited quasar sample.

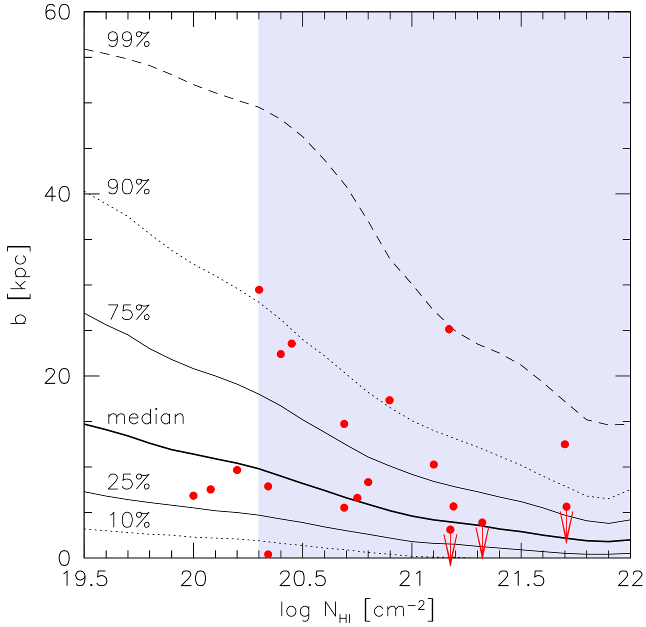

Figure 15. Conditional probability of impact parameter as a function of H I column density. The thick solid line shows the median impact parameter as calculated from our 21-cm emission-line maps. The other lines show the 10th, 25th, 75th, 90th and 99th percentiles, as indicated by the labels. The points are from DLA galaxy searches in the $z < 1$ universe.

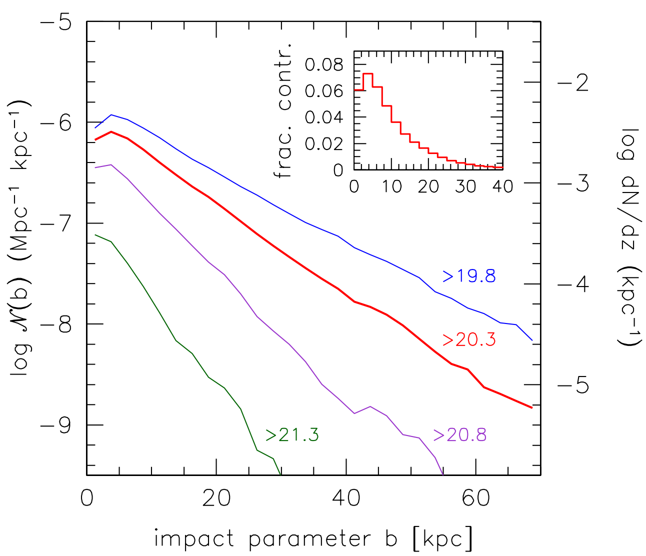

Figure 16. The probability distribution of impact parameter b between the background QSO and the centre of a galaxy giving rise to H I absorption. The lines show the product of cross-sectional area and space density, which translates to the number of expected absorbers per Mpc per kpc. The right axis shows the corresponding number of absorbers per unit redshift $\mathrm{d}N/\mathrm{d}z$. The different lines correspond to different column density limits, as indicated by the labels. The thick line corresponds to the classical DLA limit of $\log N_{\mathrm{H\,I}} > 20.3$. The inset shows the probability distribution of b for column densities $\log N_{\mathrm{H\,I}} > 20.3$ on a linear vertical scale.

A more detailed view of the distribution of impact parameters is presented in Fig. 16, which shows the predicted probability distribution of b for different column density cut-offs. The peak of the distribution for DLA column densities is at $b \sim 5$ kpc and the distribution drops rapidly towards higher values of b. The inset shows the

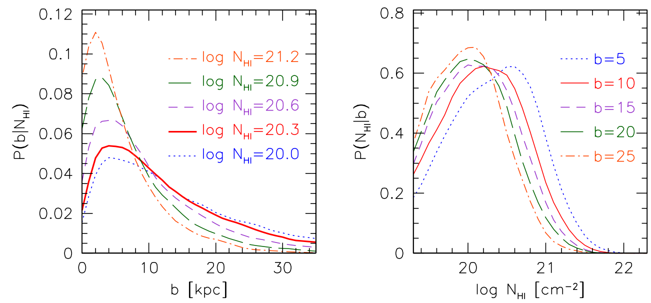

Figure 17. Left-hand panel: Normalized probability distribution of impact parameter b for different column densities. For H I column densities near the DLA limit of $2 \times 10^{20}\ \mathrm{cm}^{-2}$, the most likely impact parameter to the host galaxy is $5\,h_{75}^{-1}$ kpc. Right-hand panel: Normalized probability distribution of H I column density for different impact parameters b.

probability distribution of b above the DLA limit on a linear scale. For higher column densities, the probability distributions drop off even more rapidly, which again shows that it is extremely unlikely to encounter a high $N_{\mathrm{H\,I}}$ at a large separation from the centre of a galaxy. For DLA column densities, we find that 60 per cent of the host galaxies are expected at impact parameters <10 kpc and 32 per cent at <5 kpc. Assuming no evolution in the properties of galaxy's gas disc, these numbers imply that 37 per cent of the impact parameters are expected to be less than 1 arcsec for systems at $z = 0.5$ and 48 per cent less than 1 arcsec at $z = 1$. These numbers illustrate that very high spatial resolution imaging programs are required to successfully identify a typical DLA galaxy at $z \sim 1$.

The intrinsic assumption in this comparison is that the low-z DLA galaxy sample is a fair cross-section selected sample. In reality, the sample is a compilation of many surveys, using different selection techniques and different resolutions and wave bands to image the galaxy. Keeping this limitation in mind, we conclude that the measured impact parameters and column densities of low-z DLA galaxies is in agreement with the hypothesis that DLA galaxies can be explained by the local galaxy population.

For completeness, we show in Fig. 17 the expected probability distribution function of impact parameter b *at* various column densities. Note the difference with the previous diagrams, where we plotted probability distribution functions *above* certain column density cut-offs. The right-hand panel is the probability distribution function of column density at various values of b.

7.5 Linking DLA parameters to galaxy properties

We conclude our comparisons between DLAs and local galaxies by looking at the combined probability distribution function of column density, impact parameter and host galaxy luminosity. In Fig. 18, we again show the $N_{\mathrm{H\,I}}$ and b measurements from low-z DLA galaxies from the literature, but this time the symbol size reflects the luminosity of the galaxies such that the symbol area scales in direct proportion to L/L_*. The contours represent the probabilities that the combined measurement of $N_{\mathrm{H\,I}}$ and b is expected for a galaxy with luminosity $L > L_*$. For example, the thick solid line divides the diagram in two regions, above this line most host galaxies would be more luminous than L_*, below this line most would be less luminous than L_*. Apparently, the most luminous galaxies are most likely associated with high column density DLAs, at large impact parameters from the background QSOs.

The probability contours can be directly compared to the distribution of symbol sizes. Although the scatter is large, we see a

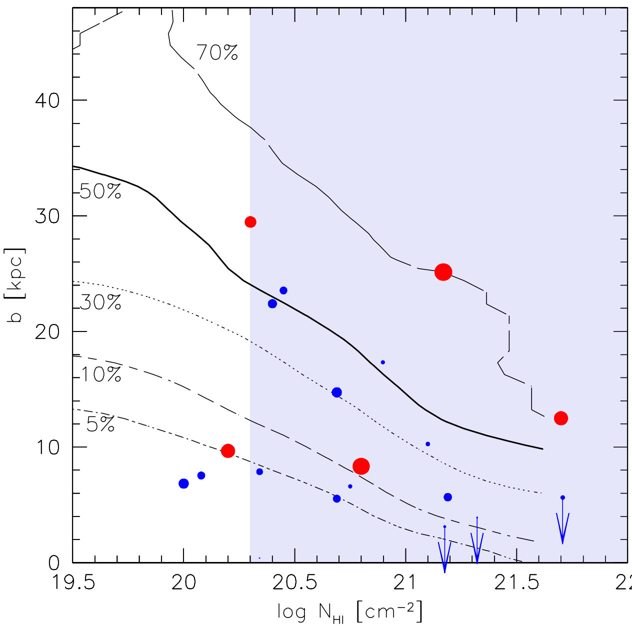

Figure 18. Probability distribution of optical luminosities of galaxies giving rise to H I absorption with column density $N_{\rm H\,I}$ and impact parameter b. The lines indicate the probability that the host galaxy is more luminous than an L_* galaxy, and represent 5, 10, 30, 50 (thick line) and 70 per cent probabilities, from bottom to top. The points are from DLA galaxy searches and are the same as in Figs 14 and 15, but here the symbol size represents intrinsic luminosity of the host galaxy. Red points indicate galaxies brighter than L_*, blue points are fainter than L_*.

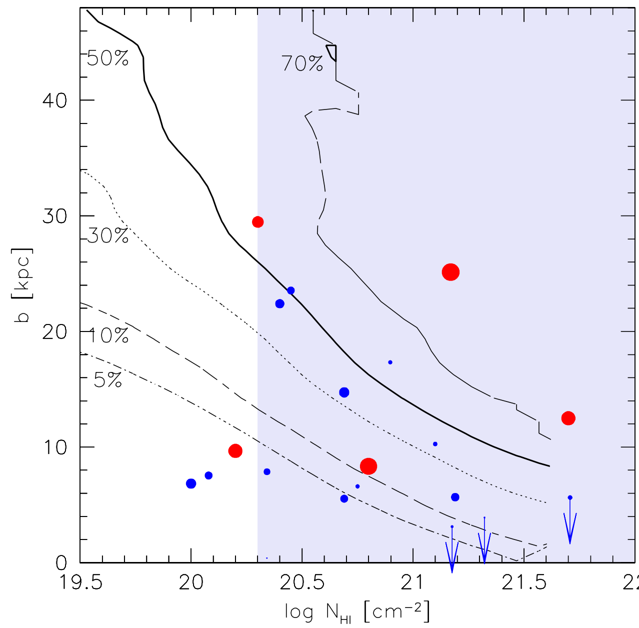

Figure 19. Probability distribution of H I masses of galaxies giving rise to H I absorption with column density $N_{\rm H\,I}$ and impact parameter b. The lines indicate the probability that the host galaxy has an H I mass in excess of $M^*_{\rm H\,I}$, and represent 5, 10, 30, 50 (thick line) and 70 per cent probabilities, from bottom to top. The points are the same as in Fig. 18.

general agreement between the points and the contours: below the 5 per cent line mostly low-luminosity galaxies are found; and on the other hand, the two galaxies above the 70 per cent line are both galaxies with high luminosities. A similar diagram is presented in Fig. 19, but here contours indicate the probability that the host galaxy has an H I mass in excess of $M^*_{\rm H\,I}$. The conclusions from this figure are very similar as those from Fig. 18.

7.6 Comparison to models and simulations of DLAs

In order to compare our findings with numbers calculated in models of galaxy formation, we first transform the B-band luminosities of our WHISP galaxies into rotational velocities via the Tully–Fisher relation.[1] We choose here to use the Tully–Fisher relation determined by Meyer et al. (in preparation) based on the HIPASS sample. Fig. 20 shows the cumulative distribution of DLA redshift number density for galaxies with different rotational velocities $V_{\rm circ}$. We present the cumulative distribution because this representation is normally used in publications based on cosmological simulations, and can therefore be directly compared to those.

On the basis of semianalytical models, Okoshi & Nagashima (2005) find that the average virial velocity of a $z = 0$ DLA is $V_{\rm vir} \sim 90$ km s^{-1} and the average luminosity is $0.05L_*$. In their models, the fraction of DLA hosts in galaxies fainter than $L_*/10$ is 98 per cent,

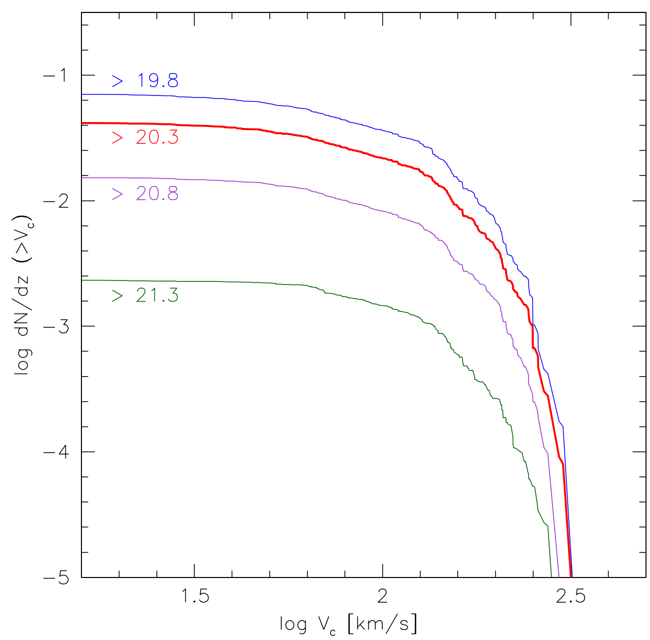

Figure 20. The cumulative redshift number density of DLAs in galaxies of different rotational velocities. The different lines correspond to different column density limits, the thick line is for log $N_{\rm H\,I} > 20.3$.

whereas we find that this fraction is only 41 per cent. Furthermore, they find that the typical impact parameter is 3 kpc, much smaller than our median value of 7.8 kpc. To make their results agree with observations of low-z DLA galaxies, Okoshi & Nagashima (2005) propose that the masking effect where the DLA galaxies are contaminated by the point spread function of the QSO hinders the

[1] In principle, a measurement of rotational velocity is available directly from the WHISP data, but at present this analysis has not been completed for the full sample. Since the observed scatter in the Tully–Fisher relation is very small, the conclusions will not change by using this approximation.

identification of 60–90 per cent of DLA galaxies with small impact parameters. The SPH simulations of Nagamine et al. (2004) also suggest that the relative contribution of low-mass galaxies to the DLA cross-section is very large: their cumulative contribution of redshift number density as a function of $V_{\rm circ}$ is steeper than what we find in Fig. 20. These authors note that the $z = 0$ results should be taken with caution because the mass resolutions that these results are based on are low and higher resolution SPH simulations are probably required to arrive at more precise results at $z = 0$. Other work, such as that of Gardner et al. (2001), Mo et al. (1998), Mo, Mao & White (1999), Haehnelt, Steinmetz & Rauch (2000) and Maller et al. (2001) mostly concentrate on the high-redshift ($z \sim 3$) DLA population and cannot be compared directly to our work, but also point to sub-L_* galaxies as the major contributors to the DLA cross-section. In conclusion, semianalytical models and cosmological simulations generally overpredict the redshift number density contribution of low-mass systems. A notable exception is the simple models of Boissier, Péroux & Pettini (2003), which show that the peak and the median of the cross-section distribution lie around L_* galaxies. These models underpredict the importance of low-mass systems, both in comparison with our results and in comparison with low-z DLA host galaxies.

From Fig. 20, we find that the mean rotational velocity $V_{\rm circ}$ of a $z = 0$ DLA is 111 km s^{-1} (the log-weighted mean $V_{\rm circ}$ is 95 km s^{-1}). Note that the rotational velocities we measure are the peak velocities of the galaxies' rotation curves, whereas in simulations galaxies are normally characterized by their virial velocity $V_{\rm vir}$. The ratio between these two values depends on the concentration index of the dark halo, but a typical value is $V_{\rm circ} \approx 1.4 V_{\rm vir}$ (see Bullock et al. 2001), which implies that the log-weighted mean virial velocity of a $z = 0$ DLA is approximately 70 km s^{-1}. Using the relation between $V_{\rm circ}$ and the virial mass $M_{\rm vir}$ given by Bullock et al. (2001), we find that the mean total mass of a $z = 0$ DLA would be $\approx 1.5 \times 10^{11}$ M$_\odot$.

8 METAL ABUNDANCES OF LOW-Z DLAS

In the previous section, we have presented evidence that DLAs arise in the gas discs of galaxies such as those in the $z = 0$ population. Measuring metallicities in DLAs therefore should provide information on abundances of the interstellar matter in galaxies. Determining DLA metallicities as a function of redshift will probe the history of metal production in galaxies over cosmic time. However, the metallicities typically measured in DLAs are low (around 1/13 solar), which is often taken as an indication that DLAs do not trace the general galaxy population, for which a mass-weighted mean metallicity of near-solar is expected at low z (see e.g. Pettini et al. 1997). In this section, we present a more detailed analysis of the expected metallicities of DLAs, under the assumption that they arise in the gas discs of normal present-day galaxies. We have no direct measurements of metal abundances for the complete sample of WHISP galaxies. However, we can make use of metallicity studies in other galaxies to statistically assign metallicities to our sample. Although this approach might introduce some degree of uncertainty in the results, it will help in understanding the observed metal abundance measurements in DLAs. It should be kept in mind that the abundances of local galaxies are measured from emission lines arising in the photoionized gas, while the measurements in DLAs are from absorption lines in the neutral gas. However, recent work by Schulte-Ladbeck et al. (2005) shows that at least in one well-studied nearby galaxy the emission and absorption measurements of the same α-elements are consistent.

8.1 The expected metallicities of DLAs at $z = 0$

We take two different approaches to assigning metallicities to our sample of galaxies. The first approach is to adopt the well-established metallicity–luminosity ($Z - L$) relation for local galaxies and apply that to our sample. We choose to adopt the relation given by Garnett (2002) for oxygen abundances:

$$\log({\rm O/H}) = -0.16 M_B - 6.4. \qquad (11)$$

The results do not change significantly if instead we use the more recent $Z - L$ relation derived from SDSS imaging and spectroscopy of 53 000 galaxies (Tremonti et al. 2004). To convert the log(O/H) values to solar values, we adopt the solar abundance of $12 + \log({\rm O/H}) = 8.66$ from Asplund et al. (2004). The effect of abundance gradients as a function of galactocentric distance is taken into account by using the result from Ferguson, Gallagher & Wyse (1998), who found a mean gradient of [O/H] of -0.09 dex kpc^{-1} along the major axes of spiral galaxies. We assume that this gradient is equal for all galaxies and that it does not vary as a function of radius. We apply a simple geometrical correction to correct for inclined discs. Furthermore, we assume that equation (11) applies to the mean abundance measurement within R_{25}, which agrees with Garnett (2002). For each galaxy in our sample, we scale the offset of the gradient such that the mean abundance measurement within R_{25} fits the metallicity–luminosity relation. This approach intrinsically assumes that the [O/H] abundance gradients are independent of galaxy luminosity. To test the effect of this assumption on the calculation of expected metallicities of DLAs, we also take a second approach in which we adopt an [O/H] gradient that has both the intercept and the slope varying with galaxy absolute magnitude. We fit straight lines to the relations found by Vila-Costas & Edmunds (1992) (their fig. 11) to find the varying slope and intercept. The two approaches depend on completely independent observations of metal abundances in local galaxies.

Every pixel in our 21-cm maps is assigned [O/H] values based on the two procedures. Applying a similar method to that set out in Section 7, we can now calculate the expected [O/H] distribution for cross-section selected samples for different column density limits. The results are shown in Fig. 21, where the solid lines refer to the first approach of fixed gradients, and the dashed lines refer to the varying gradients.

Although the distributions peak at slightly different locations, it is obvious that the global trends are not strongly dependent on our assumptions on abundance gradients in discs. The main conclusion is that the metallicity distribution for H I column densities log $N_{\rm H\,I} > 20.3$ peaks at around [O/H] $= -1$ to -0.7, much lower than the mean value of an L_* galaxy of [O/H] ≈ 0. Furthermore, we see a strong correlation between the peak of the [O/H] probability distribution and the H I column density limit: for H I column densities in excess of log $N_{\rm H\,I} = 21.3$, the expected peak of the distribution is at [O/H] $= -0.2$. This correlation is expected, since our assumed radial abundance gradients impose a relation between $N_{\rm H\,I}$ and [O/H]. Taking into account uncertainties in the H I mass function, in the $L - Z$ relation and in the abundance gradients in galaxies, we adopt a value of [O/H] $= -0.85 \pm 0.2$ as a representative value for the median cross-section weighted abundance of H I gas in the local universe above the DLA column density limit.

8.2 Comparison to low-z DLA metallicity measurements

It is interesting to compare this expected abundance of DLAs at $z = 0$ to higher redshift values to see whether the measurements can be brought into agreement. The first evidence of evolution

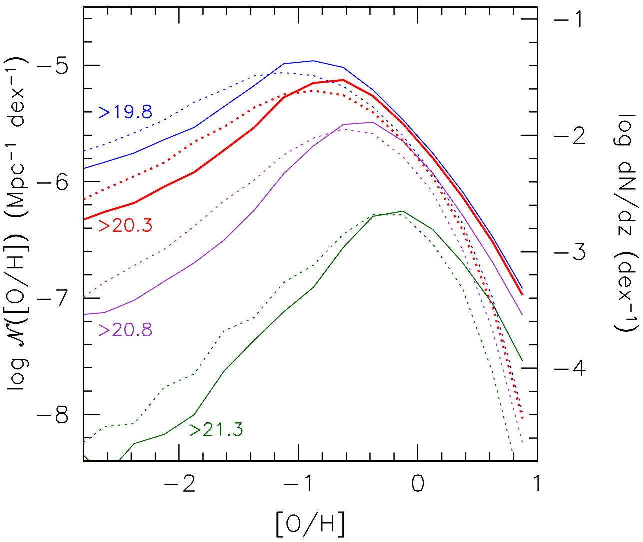

Figure 21. The probability distribution of oxygen abundance [O/H] of H I absorbers. The lines show the product of cross-sectional area and space density, which translates to the number of expected absorbers per Mpc per decade. The right axis shows the corresponding number of absorbers per unit redshift $\mathrm{d}N/\mathrm{d}z$. The solid lines refer to the approach of assuming fixed [O/H] gradients and the dashed lines refer to varying gradients (see text). The four different lines for each approach correspond to different column density limits, as indicated by the labels. The thick lines correspond to the classical DLA limit of $\log N_{\mathrm{H\,I}} > 20.3$.

in DLA metallicities over cosmic time was presented by Kulkarni & Fall (2002), contrary to previous claims of no evolution (e.g. Pettini et al. 1997, 1999). This result was further established by an analysis of 125 DLA metallicity measurements over the redshift range $0.5 < z < 5$ by Prochaska et al. (2003), who reported significant evolution of -0.26 ± 0.07 dex per unit redshift in the mean metallicity [M/H]. Kulkarni et al. (2005) compiled new metallicity measurements in four DLAs at $z < 0.52$ and combined with literature measurements this study also finds evolution in [M/H] of -0.18 ± 0.07 dex per unit redshift. The Prochaska et al. (2003) metallicity measurements are mostly based on α-element abundances, whereas the Kulkarni et al. (2005) data are mostly based on Zn abundances. We refer to Kulkarni et al. (2005) for a discussion on why Zn is an appropriate choice as a metallicity indicator.

Before we compare our $z = 0$ results to those for DLAs at higher redshifts, we discuss the different measurements of 'mean metallicity' that we can use to make the comparison. The first is to calculate the global interstellar metallicity $\bar{Z}$, defined as

$$\bar{Z} = \frac{\int N_{\mathrm{H\,I}} f(N_{\mathrm{H\,I}}) Z(N_{\mathrm{H\,I}})\, \mathrm{d}N_{\mathrm{H\,I}}}{\int N_{\mathrm{H\,I}} f(N_{\mathrm{H\,I}})\, \mathrm{d}N_{\mathrm{H\,I}}}. \qquad (12)$$

The reason that this equation gives a true measurement of the interstellar metallicity is that absorption lines are cross-section selected, which implies that a correct weighting of different regions in absorbing systems is automatically taken into account, as is stressed by Kulkarni & Fall (2002). In practice, in DLA studies $\bar{Z}$ is normally calculated by taking the average over the metallicities of individual absorption-line systems weighted by their H I column densities. For our low-z data, we can determine $\bar{Z}$ by simply taking the mass-weighted average of all mean metallicities of the WHISP galaxies:

$$\bar{Z} = \frac{\int \Theta(M_{\mathrm{H\,I}}) M_{\mathrm{H\,I}} Z(M_{\mathrm{H\,I}})\, \mathrm{d}M_{\mathrm{H\,I}}}{\int \Theta(M_{\mathrm{H\,I}}) M_{\mathrm{H\,I}}\, \mathrm{d}M_{\mathrm{H\,I}}}, \qquad (13)$$

where $\Theta(M_{\mathrm{H\,I}})$ is the H I mass function and $Z(M_{\mathrm{H\,I}})$ is the mean metallicity of a galaxy with H I mass $M_{\mathrm{H\,I}}$. We can calculate $Z(M_{\mathrm{H\,I}})$ by taking the column density-weighted metallicity of each WHISP galaxy, but only counting column densities above the DLA limit. Applying this method, we find values of $\bar{Z} = 0.58$ and $0.35\,\mathrm{Z}_\odot$ for the fixed gradient and the variable gradient method, respectively. Kulkarni & Fall (2002) and Fukugita & Peebles (2004) applied similar techniques, but integrated over the optical luminosity function and found values of $\bar{Z} \approx 0.8\,\mathrm{Z}_\odot$ and $\bar{Z} = 0.83 \pm 0.25\,\mathrm{Z}_\odot$. The reason for these values being higher than ours is that these studies use one global metallicity measurement for each galaxy (which involves some radial averaging over the inner parts of galaxies), while our analysis takes into account radial abundance gradients over the whole H I gas disc. For the mean mass-weighted metallicity of H I gas with $\log N_{\mathrm{H\,I}} > 20.3$ at $z = 0$, we adopt the value of $\log \bar{Z}/\mathrm{Z}_\odot = -0.35 \pm 0.2$, where the errors again represent all uncertainties in arriving at this result.

The second measurement of metallicity is the cross-section weighted average, which we will refer to as $\hat{Z}$. For DLAs, this measurement is simply the unweighted mean of the metallicities and represents a 'typical' metallicity of DLAs. For our $z = 0$ sample, we can make use of the calculations presented in Fig. 21, which shows the cross-section weighted [O/H] distribution of high column density H I gas in the local universe. We find values of $\hat{Z} = 0.36\,\mathrm{Z}_\odot$ and $\hat{Z} = 0.21\,\mathrm{Z}_\odot$ for the fixed gradient and the variable gradient method, respectively, and hence adopt a value of $\log \hat{Z}/\mathrm{Z}_\odot = -0.55 \pm 0.2$, for the 'typical' metallicity of $z = 0$ DLAs.

The third method stems directly from the way we presented the probability distribution of metallicity in Fig. 21. As discussed above, we derive from this the cross-section weighted median metallicity, for which we adopted $\log \tilde{Z}/\mathrm{Z}_\odot = -0.85 \pm 0.2$.

In Fig. 22, we show the metallicities in DLAs as a function of redshift, extracted from the combined compilations by Prochaska et al. (2003) and Kulkarni et al. (2005). In amalgamating the two data sets, we gave preference to Zn measurements for systems that occurred in both lists. The Kulkarni et al. (2005) data include many Zn measurements at low z, but a large fraction of those are upper limits. In order to take these limits into account appropriately, we applied the Kaplan–Meier estimator for randomly censored data sets, as implemented in the survival analysis package ASURV (Feigelson & Nelson 1985). In six different redshift bins (approximately the same as those defined by Kulkarni et al. 2005), we calculate the mean $N_{\mathrm{H\,I}}$-weighted ($\bar{Z}$), the mean cross-section weighted ($\hat{Z}$) and the median metallicities, as indicated by solid circles, triangles and stars, respectively. The error bars are 1σ statistical uncertainties as given by the Kaplan–Meier estimator. The long-dashed, short-dashed and dotted lines show the linear least-squares fits to each set of measurements. The larger symbols at $z = 0$ show our estimates of metallicities in the local universe.

For all measurements of metallicity, a slope between -0.25 and -0.3 dex per unit redshift can be seen in agreement with the findings of Prochaska et al. (2003) and Kulkarni et al. (2005), on whose compilations of data this figure is based. This increase in metallicity is consistent between the highest redshift points at $z \sim 4$ and the lowest points at $z \sim 0.6$. If we assume that DLAs arise in the gas discs of galaxies, where continued star formation causes a release of metals into the interstellar medium (ISM), it seems reasonable

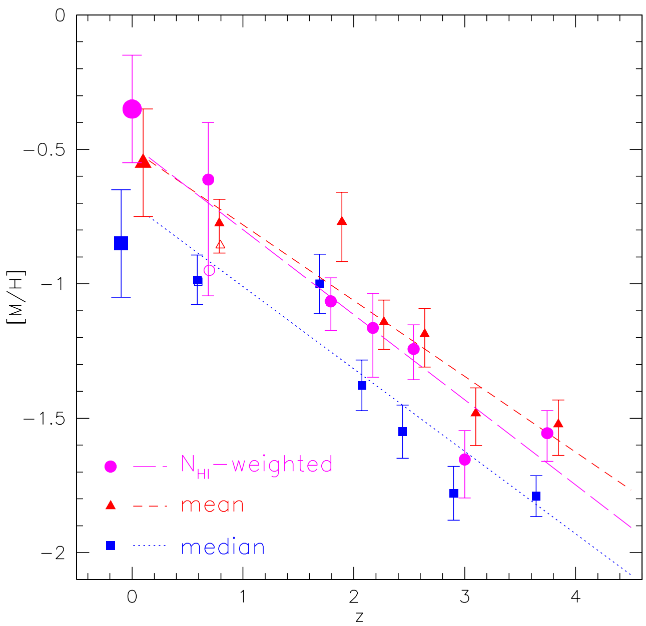

Figure 22. The metallicity [M/H] measurements in DLAs as a function of redshift. Data at redshifts $z > 0$ are taken from Prochaska et al. (2003) and Kulkarni et al. (2005). Survival analysis has been used to calculate mean and median values because the data include many upper limits. The symbols refer to column density-weighted mean (filled circles), the cross-section weighted mean (filled triangles) and median values (filled squares) in six redshift bins. The error bars indicate 1σ statistical uncertainties. The lines are least-squares fits to the $z > 0$ data points. The points at $z = 0$ are from our analysis as described in the text. The open symbols at $z \sim 0.6$ show the effect of excluding the X-ray metallicity measurement in Q0235+164. The squares and triangles are offset horizontally by −0.1 and 0.1 dex, respectively.

to assume that this evolution in metallicity persists down to $z = 0$. Note also that most models of cosmic chemical evolution predict a nearly exponential increase in metallicity as a function of redshift (cf. Kulkarni & Fall 2002). Given this assumption, we find from Fig. 22 that the expected metallicity of DLAs at $z = 0$ is in excellent agreement with our estimates from the local galaxy population: the $z = 0$ extrapolations of all three lines are within the uncertainties of our estimates.

Kulkarni et al. (2005) have argued that the $N_{\rm H\,I}$-weighted DLA metallicities do not rise up to near-solar values at $z = 0$. These authors find a DLA metal abundance of $-0.79 \pm 0.18\,{\rm Z}_\odot$ at $z = 0$ using survival analysis, a factor of 2 lower than the Prochaska et al. (2003) extrapolation. This discrepancy lies mostly in the exclusion of the X-ray absorption based metallicity of the low-z system AO 0235+164 (Junkkarinen et al. 2004). This system causes the large error bars on the $z \sim 0.6$ points in Fig. 22. The open symbols in Fig. 22 show the effect of excluding AO 0235+164. The mean and median [M/H] are not affected much, but the $N_{\rm H\,I}$-weighted value drops by more than a factor of 2 because of the high $N_{\rm H\,I}$ measured in this system. Hence, if we only used the UV absorption measurements, we would find that our $N_{\rm H\,I}$-weighted $\bar{Z}$ in galaxies is a factor of 2 higher than the extrapolated value from DLAs. Different authors disagree on whether it is fair to include this system (cf. Chen, Kennicutt & Rauch 2005; Kulkarni et al. 2005), but at least it illustrates how poor the statistics are on low-z abundance measurements. The lowest redshift bin includes 17 measurements (including AO 0235+164), of which five are limits. For illustration, if we calculate $\log \bar{Z}/{\rm Z}_\odot$ at $z = 0$ from 17 random sightlines through our galaxy sample, we find that the statistical error on this value is $-0.2 + 0.35$ dex, demonstrating that metallicity measurements based on small samples of DLAs are unavoidably marked by large uncertainties (see also Chen et al. 2005).

Interestingly, we see that for local galaxies the $N_{\rm H\,I}$-weighted $\bar{Z}$ is higher than the mean $\hat{Z}$. Although the statistics are poor, it appears that for $z > 1.5$ DLAs this is not the case. The origin of this difference might lie in the dust obscuration bias in DLAs: DLAs with the highest H I column densities and highest metallicities could be missed in magnitude-limited surveys as a consequence of their own extinction (see e.g. Fall & Pei 1989, 1993; Ellison et al. 2001; Murphy & Liske 2004; Vladilo & Péroux 2005; Wild & Hewett 2005, for a continued discussion on this issue). If, like at $z = 0$, there is an intrinsic positive correlation between $N_{\rm H\,I}$ and metallicity, this bias would have a much higher effect on the $N_{\rm H\,I}$-weighted $\bar{Z}$ than on the mean $\hat{Z}$ of DLAs, causing the two measurements to be very similar in magnitude. In our local galaxy sample, such a bias would not exist. The fact that we see a factor of 2 difference between the two values at $z = 0$ and not for $z > 1.5$ DLAs therefore is suggestive of dust obscuration introducing biases in DLA samples.

Finally, we comment on the scatter in the observed metallicity measurements in DLAs. From the probability distribution of [O/H] in Fig. 21, we find that the expected 1σ scatter in cross-section selected metallicity measurements is 0.7 dex. A similar value is estimated by Chen et al. (2005). This is slightly larger than the typical scatter observed in metallicity measurements at high redshift of ∼0.5 dex, illustrating that metallicity gradients in galaxy discs can easily explain the observed scatter in DLA metallicity measurements.

In conclusion, we find that the cross-section weighted mean metallicity of local galaxies as well as the mass-weighted metallicity is in very good agreement with the hypothesis that DLAs arise in the H I discs of galaxies, provided that the metallicities in DLAs continue to evolve since $z = 0.5$ with a rate similar to that observed between $z = 0.5$ and 4.

Before ending this section, we wish to comment briefly on the work of Chen et al. (2005), who presented similar conclusions based on Monte Carlo simulations. These authors use average radial H I profiles for three types of galaxies and assume that the metallicity gradients in these galaxies are similar to what is found for their sample of DLAs. Their analysis does not take into account that galaxies over a large range in absolute magnitude contribute to the DLA cross-section (see Section 7.1), and effectively, only L_* galaxies are considered. Therefore, the $L - Z$ relation is not taken into account in this analysis. Furthermore, in their analysis, the mean metallicity is measured over the whole gas disc out to the radius where 21-cm emission is normally detected, and not just over the region $\log N_{\rm H\,I} > 20.3$. Since there is an intrinsic relation between $N_{\rm H\,I}$ and metallicity, this causes an underestimation of the mean Z for DLAs. This explains why the Chen et al. (2005) estimate of the $N_{\rm H\,I}$-weighted mean $\bar{Z} = 0.3\,{\rm Z}_\odot$ is lower than our estimate.

9 CONCLUSIONS

In this paper, we tested the hypothesis that DLA absorption lines observed in the spectra of background QSOs arise in gas discs of galaxies like those in the $z = 0$ population. Since the H I column densities seen in DLAs ($N_{\rm H\,I} > 2 \times 10^{20}$) are the same as those routinely observed in 21-cm emission-line studies of local galaxies, we can make use of these observations to test the hypothesis. Thus, we used a sample of 355 high-quality WSRT 21-cm emission-line maps to calculate in detail the expected column density distribution function, the redshift number density and the expected probability distribution functions of different galaxy parameters of the low-z DLAs. We summarize the conclusions as follows:

(i) The local galaxy population can explain the incidence rate of low-z DLAs. There appears to be no evolution in the 'cross-section times space density' or the mean free path between absorbers from $z \sim 1.5$ to $z = 0$. Between the highest redshifts at which DLAs are found ($z \sim 4$–5) and the present time, the evolution in comoving incidence rate is only approximately a factor of 2. We find that $\mathrm{d}N/\mathrm{d}z(z = 0) = 0.045 \pm 0.006$.

(ii) Based on the local galaxy population, it is expected that the DLA cross-section is dominated by sub-L_* galaxies (87 per cent). This agrees with the statistics of identified DLA host galaxies at low z. 50 per cent of the low-z DLAs should arise in galaxies with H I masses less than $M^*_{\rm H\,I} = 6 \times 10^9\,\mathrm{M}_\odot$. The median $z = 0$ DLA arises in a $L_*/7$ galaxy with an H I mass of $2 \times 10^9\,\mathrm{M}_\odot$.

(iii) The distribution of impact parameters and column densities agrees very well between local galaxies and low-z DLA galaxies. The median impact parameter between the line of sight to a QSO and the centre of the galaxy giving rise to a DLA is 7.8 kpc. For systems at $z = 0.5$ ($z = 1$), we expect that 37 per cent (48 per cent) have impact parameters less than 1 arcsec. These findings support indications that optical surveys for DLA host galaxies miss identifications at very small impact parameters, because of the brightness of the QSO or because of blending due to too low spatial resolution. If obscuration of background QSOs by dust in DLA galaxies is important, this might also have the strongest effect at small impact parameters.

(iv) We combine our data set with the well-established luminosity–metallicity relation of galaxies and observed metallicity gradients in galaxy discs to estimate the expected metallicity distribution of low-z DLAs. We find that the expected median metallicity of $z = 0$ DLAs is approximately 1/7 solar, in good agreement with observations of metal lines in DLAs. The mean mass-weighted metallicity of the interstellar matter in local galaxies above the DLA limit is approximately half solar. This is consistent with extrapolations from higher redshift measurements, although the $z = 0$ extrapolated value has large uncertainties given the poor statistics from DLAs with redshifts approximately $z \approx 1.5$.

(v) The column density distribution function $f(N_{\rm H\,I})$ in the local universe can be fitted satisfactorily with a gamma distribution. A single power law is not a good fit. There is remarkably little evolution in the shape of $f(N_{\rm H\,I})$ from high z to the present.

(vi) Most (≈81 per cent) of the cosmological mass density in H I at $z = 0$ is locked up in column densities above the classical DLA limit of $N_{\rm H\,I} > 2 \times 10^{20}\,\mathrm{cm}^{-2}$, the rest is mostly in column densities just below this limit. The fraction is consistent over the redshift range $z \sim 5$ to $z = 0$.

ACKNOWLEDGMENTS

This work benefited from discussions with Nicolas Bouché, Céline Péroux, Mike Fall, Palle Møller and Jochen Liske on the nature of DLAs. We also thank them and the anonymous referee for useful comments on the manuscript. We are grateful to Sandhya Rao and Jason Prochaska for communicating results before publication. JMvdH acknowledges support from ATNF for a distinguished visitor grant. The WSRT is operated by The Netherlands Foundation for Research in Astronomy (ASTRON) with financial support from The Netherlands Organisation for Scientific Research (NWO). We have made use of the LEDA data base (http://leda.univ-lyon1.fr). This research has made use of the NASA/IPAC Extragalactic Data base (NED) which is operated by the Jet Propulsion Laboratory, California Institute of Technology, under contract with the National Aeronautics and Space Administration.

REFERENCES

Asplund M., Grevesse N., Sauval A. J., Allende Prieto C., Kiselman D., 2004, A&A, 417, 751
Boissier S., Péroux C., Pettini M., 2003, MNRAS, 338, 131
Bouché N., Lowenthal J. D., Charlton J. C., Bershady M. A., Churchill C. W., Steidel C. C., 2001, ApJ, 550, 585
Bowen D. V., Huchtmeier W., Brinks E., Tripp T. M., Jenkins E. B., 2001, A&A, 372, 820
Bowen D. V., Tripp T. M., Jenkins E. B., 2001, AJ, 121, 1456
Braun R., Thilker D. A., 2004, A&A, 417, 421
Broeils A. H., 1992, PhD thesis, Univ. Groningen
Bullock J. S., Kolatt T. S., Sigad Y., Somerville R. S., Kravtsov A. V., Klypin A. A., Primack J. R., Dekel A., 2001, MNRAS, 321, 559
Burbidge G., Odell S. L., Roberts D. H., Smith H. E., 1977, ApJ, 218, 33
Burbidge E. M., Beaver E. A., Cohen R. D., Junkkarinen V. T., Lyons R. W., 1996, AJ, 112, 2533
Busswell G. S., Shanks T., Frith W. J., Outram P. J., Metcalfe N., Fong R., 2004, MNRAS, 354, 991
Carilli C. L., Rawlings S., 2004, New Astrophys. Rev., 48, 979
Chen H., Lanzetta K. M., 2003, ApJ, 597, 706
Chen H.-W., Kennicutt R. C., Rauch M., 2005, ApJ, 620, 703
Chengalur J. N., Kanekar N., 2002, A&A, 388, 383
Churchill C. W., 2001, ApJ, 560, 92
Colbert J. W., Malkan M. A., 2002, ApJ, 566, 51
Cole S. et al., 2001, MNRAS, 326, 255
Corbelli E., Bandiera R., 2002, ApJ, 567, 712
Corbelli E., Salpeter E. E., 1993, ApJ, 419, 104
Cross N., Driver S. P., 2002, MNRAS, 329, 579
Curran S. J., Webb J. K., Murphy M. T., Bandiera R., Corbelli E., Flambaum V. V., 2002, Publ. Astron. Soc. Austr., 19, 455
de Blok W. J. G., McGaugh S. S., 1997, MNRAS, 290, 533
Dessauges-Zavadsky M., Péroux C., Kim T.-S., D'Odorico S., McMahon R. G., 2003, MNRAS, 345, 447
Dickey J. M., Lockman F. J., 1990, ARA&A, 28, 215
Ellison S. L., Yan, L., Hook I. M., Pettini M., Wall J. V., Shaver P., 2001, A&A, 379, 393
Fall S. M., Pei Y. C., 1989, ApJ, 337, 7
Fall S. M., Pei Y. C., 1993, ApJ, 402, 479
Feigelson E. D., Nelson P. I., 1985, ApJ, 293, 192
Ferguson A. M. N., Gallagher J. S., Wyse R. F. G., 1998, AJ, 116, 673
Frith W. J., Busswell G. S., Fong R., Metcalfe N., Shanks T., 2003, MNRAS, 345, 1049
Fukugita M., Peebles P. J. E., 2004, ApJ, 616, 643
Fynbo J. U., Møller P., Warren S. J., 1999, MNRAS, 305, 849
Gardner J. P., Katz N., Hernquist L., Weinberg D. H., 2001, ApJ, 559, 131
Garnett D. R., 2002, ApJ, 581, 1019
Haehnelt M. G., Steinmetz M., Rauch M., 1998, ApJ, 495, 647
Haehnelt M. G., Steinmetz M., Rauch M., 2000, ApJ, 534, 594
Hopkins A. M., 2004, ApJ, 615, 209
Junkkarinen V. T., Cohen R. D., Beaver E. A., Burbidge E. M., Lyons R. W., Madejski G., 2004, ApJ, 614, 658
Kanekar N., Chengalur J. N., Subrahmanyan R., Petitjean P., 2001, A&A, 367, 46
Kauffmann G., 1996, MNRAS, 281, 475
Khersonsky V. K., Turnshek D. A., 1996, ApJ, 471, 657
Kulkarni V. P., Fall S. M., 2002, ApJ, 580, 732
Kulkarni V. P., Hill J. M., Schneider G., Weymann R. J., Storrie-Lombardi L. J., Rieke M. J., Thompson R. I., Jannuzi B. T., 2000, ApJ, 536, 36
Kulkarni V. P., Fall S. M., Lauroesch J. T., York D. G., Welty D. E., Khare P., Truran J. W., 2005, ApJ, 618, 68
Lacy M., Becker R. H., Storrie-Lombardi L. J., Gregg M. D., Urrutia T., White R. L., 2003, AJ, 126, 2230

Lane W., Smette A., Briggs F., Rao S., Turnshek D., Meylan G., 1998, AJ, 116, 26
Lane W. M., Briggs F. H., Smette A., 2000, ApJ, 532, 146
Lanzetta K. M., McMahon R. G., Wolfe A. M., Turnshek D. A., Hazard C., Lu L., 1991, ApJS, 77, 1
Le Brun V., Bergeron J., Boisse P., Deharveng J. M., 1997, A&A, 321, 733
Ledoux C., Petitjean P., Bergeron J., Wampler E. J., Srianand R., 1998, A&A, 337, 51
Lin H., Kirshner R. P., Shectman S. A., Landy S. D., Oemler A., Tucker D. L., Schechter P. L., 1996, ApJ, 464, 60
Liske J., Lemon D. J., Driver S. P., Cross N. J. G., Couch W. J., 2003, MNRAS, 344, 307
Maller A. H., Prochaska J. X., Somerville R. S., Primack J. R., 2001, MNRAS, 326, 1475
Maloney P., 1993, ApJ, 414, 41
Meyer M. J. et al., 2004, MNRAS, 350, 1195
Milgrom M., 1988, A&A, 202, L9
Miller E. D., Knezek P. M., Bregman J. N., 1999, ApJ, 510, L95
Minchin R. F. et al., 2004, MNRAS, 355, 1303
Mo H. J., Mao S., White S. D. M., 1998, MNRAS, 295, 319
Mo H. J., Mao S., White S. D. M., 1999, MNRAS, 304, 175
Møller P., Warren S. J., Fall S. M., Fynbo J. U., Jakobsen P., 2002, ApJ, 574, 51
Murphy M. T., Liske J., 2004, MNRAS, 354, L31
Nagamine K., Springel V., Hernquist L., 2004, MNRAS, 348, 421
Nilson P., 1973, Uppsala General Catalogue of Galaxies. Nova Acta Regiae Soc. Scient Uppsaliensis, Ser. V, A, Vol. 1
Noordermeer E., van der Hulst J. M., Sancisi R., Swaters R., 2004, IAUS, 220, 287
Noordermeer E., van der Hulst J. M., Sancisi R., Swaters R., van Albada T. S., 2005, A&A, 442, 137
Norberg P. et al., 2002, MNRAS, 336, 907
Okoshi K., Nagashima M., 2005, ApJ, 623, 99
Pei Y. C., Fall S. M., 1995, ApJ, 454, 69
Péroux C., Storrie-Lombardi L. J., McMahon R. G., Irwin M., Hook I. M., 2001, AJ, 121, 1799
Péroux C., Irwin M. J., McMahon R. G., Storrie-Lombardi L. J., 2002, ASP Conf. Ser. Vol. 253, Chemical Enrichment of Intracluster and Intergalactic Medium. Astron. Soc. Pac., San Francisco, p. 501
Péroux C., McMahon R. G., Storrie-Lombardi L. J., Irwin M. J., 2003, MNRAS, 346, 1103
Péroux C., Deharveng J., Le Brun V., Cristiani S., 2004, MNRAS, 352, 1291
Péroux C., Dessauges-Zavadsky M., D'Odorico S., Kim T., McMahon R. G., 2005, MNRAS, 363, 479
Petitjean P., Theodore B., Smette, A., Lespine Y., 1996, A&A, 313, L25
Pettini M., Smith L. J., King D. L., Hunstead R. W., 1997, ApJ, 486, 665
Pettini M., Ellison S. L., Steidel C. C., Bowen D. V., 1999, ApJ, 510, 576
Pettini M., Ellison S. L., Steidel C. C., Shapley A. E., Bowen D. V., 2000, ApJ, 532, 65
Prochaska, J. X., Herbert-Fort S., 2004, PASP, 116, 622
Prochaska J. X., Wolfe A. M., 1997, ApJ, 487, 73
Prochaska J. X., Wolfe A. M., 1998, ApJ, 507, 113
Prochaska J. X., Gawiser E., Wolfe A. M., Quirrenbach A., Lanzetta K. M., Chen H., Cooke J., Yahata N., 2002, AJ, 123, 2206
Prochaska J. X., Gawiser E., Wolfe A. M., Castro S., Djorgovski S. G., 2003, ApJ, 595, L9
Prochaska J. X., Herbert-Fort S., Wolfe A. M., 2005, ApJ, in press
Rao S., Briggs F., 1993, ApJ, 419, 515
Rao S. M., Turnshek D. A., 2000, ApJS, 130, 1
Rao S. M., Nestor D. B., Turnshek D. A., Lane W. M., Monier E. M., Bergeron J., 2003, ApJ, 595, 94
Rao S. M., Turnshek D. A., Nestor D. B., 2005, ApJ, in press (astro-ph/0509469)
Rosenberg J. L., Schneider S. E., 2002, ApJ, 567, 247
Rosenberg, J. L., Schneider S. E., 2003, ApJ, 585, 256
Ryan-Weber E. V., Webster R. L., Staveley-Smith L., 2003, MNRAS, 343, 1195
Ryan-Weber E. V., Webster R. L., Staveley-Smith L., 2005a, MNRAS, 356, 1600
Ryan-Weber E. V., Staveley-Smith L., Webster R. L., 2005b, MNRAS, in press
Schaye J., 2001, ApJ, 559, L1
Schulte-Ladbeck R. E., König B., Miller C. J., Hopkins A. M., Drozdovsky I. O., Turnshek D. A., Hopp U., 2005, ApJ, 625, 79
Steidel C. C., Dickinson M., Meyer D. M., Adelberger K. L., Sembach K. R., 1997, ApJ, 480, 568
Storrie-Lombardi L. J., Wolfe A. M., 2000, ApJ, 543, 552
Storrie-Lombardi L. J., Irwin M. J., McMahon R. G., 1996, MNRAS, 282, 1330
Swaters R. A., van Albada T. S., van der Hulst J. M., Sancisi R., 2002, A&A, 390, 829
Tammann G. A., 1985, in Kunth D., Thuan T. X., Tran Thanh Van J., eds, Star-Forming Dwarf Galaxies and Related Objects. Editions Frontières, Gif-sur-Yvette, p. 41
Tremonti C. A. et al., 2004, ApJ, 613, 898
Turnshek D. A., Rao S., Nestor D., Lane W., Monier E., Bergeron J., Smette A., 2001, ApJ, 553, 288
Tytler D., 1987, ApJ, 321, 49
van der Hulst J. M., van Albada T. S., Sancisi R., 2001, ASP Conf. Ser. Vol. 240, Gas and Galaxy Evolution, Astron. Soc. Pac., San Francisco, p. 451
Verheijen, M. A. W., Sancisi R., 2001, A&A, 370, 765
Vila-Costas M. B., Edmunds M. G., 1992, MNRAS, 259, 121
Vladilo G., Péroux C. 2005, A&A, in press
Warren S. J., Møller P., Fall S. M., Jakobsen P., 2001, MNRAS, 326, 759
Wild V., Hewett P. C., 2005, MNRAS, 361, L30
Wolfe A. M., Turnshek D. A., Smith H. E., Cohen R. D., 1986, ApJS, 61, 249
Wolfe A. M., Lanzetta K. M., Foltz C. B., Chaffee F. H., 1995, ApJ, 454, 698
Wyithe J. S. B., Agol E., Fluke C. J., 2002, MNRAS, 331, 1041
Zwaan M. A., 2000, PhD Thesis, University of Groningen
Zwaan M. A., Briggs F. H., Sprayberry D., Sorar E., 1997, ApJ, 490, 173
Zwaan, M. A., Verheijen M. A. W., Briggs F. H., 1999, Pub. Astron. Soc. Aust., 16, 100
Zwaan M., Briggs F. H., Verheijen M., 2002, ASP Conf. Ser. Vol. 254, Extragalactic Gas at Low Redshift, Astron. Soc. Pac., San Francisco, p. 169
Zwaan M. A. et al., 2003, AJ, 125, 2842
Zwaan M. A., Meyer M. J., Staveley-Smith L., Webster R. L., 2005, MNRAS, 359, L30

This paper has been typeset from a TEX/LATEX file prepared by the author.